Geochemical composition of Trondheimsfjord surface sediments: Sources and spatial variability of marine and terrigenous components

Johan C. Faust [a, b, *], Jochen Knies [a], Trond Slagstad [a], Christoph Vogt [c], Gesa Milzer [d], Jacques Giraudeau [d]

[a] Geological Survey of Norway, 7491 Trondheim, Norway
[b] University of Tromsø, Department of Geology, 9011 Tromsø, Norway
[c] Crystallography/ZEKAM, Geosciences, University of Bremen, 28334 Bremen, Germany
[d] Universite Bordeaux 1 UMR CNRS 5805 EPOC, 33405 Talence cedex , France

*Corresponding author: Norges geologiske undersøkelse /Geological Survey of Norway (NGU), Marine Geology, Postboks 6315 Sluppen, 7491 Trondheim, Norway. Tel.: +47 7390 4000. E-mail address: jfaust@uni-bremen.de (J. Faust).

Keywords: Trondheimsfjord, surface sediments, Norway, fjord environment, stable isotopes, carbon, nitrogen, elemental composition, terrigenous input, marine input, inorganic organic geochemistry

Abstract

High sedimentation rates in fjords provide excellent possibilities for high resolution sedimentary and geochemical records over the Holocene. As a baseline for an improved interpretation of geochemical data from fjord sediment cores, this study aims to investigate the inorganic/organic geochemistry of surface sediments and to identify geochemical proxies for terrestrial input and river discharge in the Trondheimsfjord, central Norway. Sixty evenly distributed surface sediment samples were analysed for their elemental composition, total organic carbon (C_{org}), nitrogen (N_{org}) and organic carbon stable isotopes ($\delta^{13}C_{org}$), bulk mineral composition and grain size distribution. Our results indicate carbonate marine productivity to be the main $CaCO_3$ source. Also, a strong decreasing gradient of marine-derived organic matter from the entrance towards the fjord inner part is consistent with modern primary production data. We show that the origin of the organic matter as well as the distribution of $CaCO_3$ in Trondheimsfjord sediments can be used as a proxy for the variable inflow of Atlantic water and changes in river runoff. Furthermore, the comparison of

grain size independent Al-based trace element ratios with geochemical analysis from terrigenous sediments and bedrocks provides evidence that the distribution of K/Al, Ni/Al and K/Ni in the fjord sediments reflect regional sources of K and Ni in the northern and southern drainage basin of the Trondheimsfjord. Applying these findings to temporally well-constrained sediment records will provide important insights into both the palaeoenvironmental changes of the hinterland and the palaeoceanographic modifications in the Norwegian Sea as response to rapid climate changes and associated feedback mechanisms.

1. Introduction

In general, fjords are ideal places to study modern and past environmental and climate changes (Syvitski et al., 1987). The sediments delivered to fjords contain information regarding environmental changes of the hinterland and oceanographic variability on the adjacent continental margins and shelves through water mass exchange (e.g. Schafer et al., 1983; Syvitski and Schafer, 1985; Howe et al., 2010). Moreover, biogenic sedimentation generated in-situ in the fjord through biogeochemical processes and primary productivity can also reflect local and global influences on the environment. As such, sediments accumulating in fjords offer an excellent opportunity for studying land-ocean interactions and can provide ultra-high-resolution records of local responses to short-term variability in the earth's climate.

Before deciphering the past climate signals in the sedimentary record, however, it is important to understand the modern depositional environment within the fjords (Inall and Gillibrand, 2010). Here, we investigate the environmental constraints in the

Trondheimsfjord, central Norway, based on sixty surface sediment samples from the entire Trondheimsfjord (Fig. 1). We used these samples to study the modern geochemical and sedimentological processes that occur within the fjord and to identify possible proxies for past environmental changes. For these purposes, we analysed all surface sediment samples for elemental composition, total organic carbon (C_{org}) and total organic nitrogen (N_{org}) content, organic carbon stable isotopes ($\delta^{13}C_{org}$), bulk mineral composition and grain size distribution. To the best of our knowledge, no similar systematic organic and inorganic geochemical investigation of fjord surface sediments as a basis for long term palaeoclimate studies has been conducted in the Trondheimsfjord or in any other Norwegian fjord.

To gain a better understanding of the modern environmental system, numerous studies have focused on the contribution of organic carbon (e.g. Sargent et al., 1983; Goñi et al., 1997; Winkelmann and Knies, 2005; Knies and Martinez, 2009) and trace elements (Hirst, 1962; Calvert et al., 1993; Hayes, 1993; Cho et al., 1999; Karageorgis et al., 2005; Govin et al., 2012) to identify marine/terrigenous sources of shelf and open ocean surface sediments. In particular, Sepúlveda et al. (2011) and Bertrand et al. (2012) conducted inorganic and organic geochemical surveys on surface sediments obtained from fjords in northern Patagonia, Chile. They reported a significant influence from freshwater inflow on their geochemical composition and a decreasing gradient of terrigenous-derived organic- and inorganic material from the inner fjords towards the open ocean. Further, Sepúlveda et al. (2011) and Bertrand et al. (2012) argued that fjords may be an important CO_2 sink and that Al-based elemental ratios are suitable proxies for estimating temporal variations in river discharge. In the current study, we took a high spatial surface sediment sample distribution and combined our results with geochemical and geological field mapping datasets from the

drainage area of the Trondheimsfjord. We aim to detect sources of particular sediment components and to better identify environmental mechanisms controlling their supply and distribution in the Trondheimsfjord. Further, by using this multiproxy approach to obtain a better understanding of the modern environmental conditions in the Trondheimsfjord area, new baseline knowledge is provided for future applications on Holocene sequences to reconstruct the variability of the North Atlantic Oscillation (NAO) and the North Atlantic Current (NAC) for the last 10,000 years.

2. Study area

The temperate Trondheimsfjord is located in the central part of Norway (Fig.1) and, with a length of approximately 135 km, it is the third longest fjord in the country (Jacobson, 1983). Like many fjords, its complex morphology is characterised by relatively wide and shallow areas, narrow trenches and steep slopes, up to 30-40 degrees (Bøe et al., 2003). Three sills, the Agdenes Sill at the entrance (max. 330 m water depth), the Tautra Ridge in the middle section (max. 100 m water depth) and the Skarnsund in the inner part (max. water depth 100 m) divide the Trondheimsfjord into four main basins: Stjørnfjord, Seaward basin, Middle fjord and Beistadfjord (Fig. 1) (For detailed maps of bathymetry and topography of the drainage area, we refer to http://kart.statkart.no). The average tide in the Trondheimsfjord is 1.8 m, the average water depth is 165 m and the maximum water depth (620 m) is found at the mouth of the Seaward basin (Sakshaug and Sneli, 2000 and references therein).

The maritime climate in the Trondheimsfjord region is strongly influenced by the NAO (Wanner et al., 2001), causing warm and wet (+NAO) or cold and dry (-NAO) weather

conditions especially during winter times. The Atlantic water flowing into Trondheimsfjord display temperatures and salinity of approximately 7.5°C and 34.8, respectively, around the entire year (Sakshaug and Sneli, 2000). It modulates seasonal air temperatures over the fjord region, resulting in lower (higher) air temperatures in summer (winter) and a strong temperature gradient from the fjord towards the hinterland is observed, especially during winter months. The total drainage area is approximately 20 000 km^2 (Rise et al., 2006) with a mean precipitation in the north-west area (1700 mm/year) that is twice as high as in the south-east region (855 mm/year). Glaciers are not present in the drainage area and the annual precipitation is strongly correlated to the river discharge (Sakshaug and Sneli, 2000) of the six main rivers enter into the fjord: Gaula, Orkla, Nidelva, Stjørdalselva, Verdalselva and Steinkjerelva (Fig. 1). The freshwater supply from these rivers decreases the surface salinity and initiates an estuarine circulation, which is a typical surface circulation system for fjords (Jacobson, 1983). The Coriolis effect deflects surface currents towards the right, especially in the Seaward basin. Ocean water entering the fjord, therefore, always flows along the south side of the fjord, while outward currents always flow along the north side (Fig. 1). As a result large volumes of the riverine water recirculate and mix into each basin before leaving the Trondheimsfjord after a residence time of ca. 20 days (Jacobson, 1983). Although the fjord is partly very deep, the water masses below the estuarine circulation cell can be described as an energetically relatively low environment and the distributions of sediments within the fjord are, therefore, largely controlled by the circulation in the upper part of the water column (Wendelbo, 1970; Syvitski, 1989). Deeper water masses are usually renewed twice a year (Jacobson, 1983) and there is no observation of sub- or anoxic conditions in the fjord.

The geology in the Trondheimsfjord region (Fig. 2) is characterized by Caledonian nappes along its southeastern side, autochthonous Precambrian granitoid gneisses and Caledonian slivers along its northwestern side, and a basement window (Tømmerås anticline) exposing Precambrian volcanic rocks near its northeastern end (Roberts, 1997). The Caledonian nappes belong to the Middle and Upper Allochthon and consist mainly of schist, metagreywacke and ophiolitic greenstone, intruded by gabbroic to tonalitic rocks. During the Quaternary, glaciers eroded deeply into the bedrock, forming a 1100-1300 m deep basin between Trondheim and the Agdenes sill (Rise et al., 2006). The hemipelagic sediments of mostly pre-Holocene age have a maximum thickness of up to 750 m (Bøe et al., 2003; Rise et al., 2006). Moreover, numerous slide and debris flow events have affected the fjord during the Holocene (Bøe et al., 2003; Bøe et al., 2004; Lyså et al., 2008; L'Heureux et al., 2009; L'Heureux et al., 2010; Hansen et al., 2011; L'Heureux et al., 2011).

3. Material and Methods

3.1 Fjord surface sediments: Sampling and preparation

In April 2011, sixty surface sediment samples were collected at water depths between 25 and 605 m across the entire Trondheimsfjord (63°40´N, 09°45´E, 64°45´N, 11°30´E) (Fig. 1 and Tab. S1). The first centimetre of multicores (5.5 cm diameter) collected from each sampling location was sampled aboard the research vessel "FF Seisma" and stored in plastic bags at -18°C. Prior to further analyses, all samples were freeze-dried and, except for grain size measurements, homogenised through grinding using a Fritsch Micro Mill PULVERISETTE 7 with agate grinding bowls and balls for 1-2 minutes at a speed of 250 rotations per minute.

3.2. Organic carbon, bulk elemental geochemistry and grain size analyses

35 elements (Al, Ti, Na, Mg, Ba, Ca, Zr, Ni, Fe, Cu, Pb, Sr, Zn, Ag, Co, Mn, As, U, Th, Cd, Sb, Bi, V, P, La, Cr, K, W, Sn, Y, Nb, Mo, Be, Sc, S) were analysed at the ACME Ltd laboratory in Vancouver, British Columbia Canada. Determination was performed by inductively coupled plasma atomic emission spectroscopy (ICP-AES) following a four-acid digestion which is considered to be a total digestion method. 250 mg of each sample is heated (200°C) in a mixture of H_2O-HF-$HClO_4$-HNO_3 (2:2:1:1) to fuming and taken to dryness. The residue is dissolved in hydrochloric acid (50 %). The analytical quality was calculated by duplicate analyses of every 20 samples (Tab. S1) and further controlled by using the certified multi-element soil standard OREAS 45e and the certified multi-element basalt standard OREAS 24p.

Analyses for total carbon (TC), total organic carbon (C_{org}) and grain size were performed at the Laboratory of the Geological Survey of Norway (NGU). Weight percentages (wt. %) of C_{org} and TC were determined with a LECO SC-444 (Tab. S2). Prior to the analysis for C_{org}, sediment subsamples (ca. 200 mg) were transferred into carbon-free pervious ceramic combustion boats. To remove inorganic carbon (carbonate) combustion boats were placed on a heating plate with 50°C (±5°C) and samples were treated with 10 % (vol.) hydrochloric acid (HCl). Subsequently, samples were rinsed 10 times with distilled water (water was withdrawn by vacuum attached to the combustion boats). The certified reference material Leco 501-034, blanks and sample replicates were included in every batch. Results are given in weight percentage and the analytical error for TC and TOC was ±2.3 % rel. (n = 28) and ±2.0 % rel. (n = 26), respectively. Carbonate content was calculated as $CaCO_3 = (TC - C_{org}) \times 8.33$. The determination of grain size distribution was performed by laser diffraction

using a Coulter LS 200 instrument. The analysis was carried out on material within a particle diameter range of 0.4–2000 µm and the results are presented on the basis of volume, as cumulative volume percentage (Tab. S3). Prior to the grain size analyses, sediment samples (0.12-0.58 g) were treated with 5 % sodium pyrophosphate ($Na_4P_4O_7 \bullet 10H_2O$, Merck PA) to prevent particles becoming charged and agglomerated and afterwards placed in an ultrasonic bath (5-6 min). At least one duplicate of each sample with the same net weight were analysed and the uncertainty was ±10% cumulative mass volume percentage. We assume biogenic silica and $CaCO_3$ to have only a minor effect on the grain size measurement because: (a) Biogenic silica analysis of 10 surface sediments from the Trondheimsfjord applying the method from Mortlock and Froelich (1989) (unpublished data, Geological Survey of Norway) reveal very low content of biogenic silica (< 0.8 %). (b) The grain size distribution is consistent with previous studies (e.g. Bøe et al., 2004) and our own observation during sampling. Furthermore, (c) the $CaCO_3$ content in 73 % of all samples within the Trondheimsfjord reveal values lower than 4.5 wt. % of the total sediment.

3.3. Total nitrogen and stable carbon isotope analyses

Total nitrogen (N_{tot} in wt%) was determined using a Carlo Erba NC2500 Isoprime elemental analyzer isotope ratio mass spectrometer (EA-IRMS) at EPOC, CNRS/University of Bordeaux 1, France. Duplicate measurements of all samples and additional triple measurements of ~25% of all samples produced a standard deviation of 0.002 % for N_{tot} (sigma 1, n = 60). The inorganic nitrogen (N_{inorg}) content was analysed on 20 mg sediment subsamples treated with KOBr-KOH solution to remove organic nitrogen (see Knies et al. (2007) for details) using an EA-IRMS (Iso-Analytical Ltd., UK). Precision of the measurement was 3.48 % (n = 10). The organic proportion of the total nitrogen content was calculated by

subtracting the N_{inorg} fraction from N_{tot}. The results from the nitrogen analyses are shown in the supplementary information Tab. S2.

Stable carbon isotopes of the C_{org} fraction ($\delta^{13}C_{org}$) were measured on decarbonated (10 % HCl) aliquots using an EA-IRMS (Iso-Analytical Ltd., UK). $\delta^{13}C_{org}$ values are given in per mil vs. Vienna-PDB (Tab. S2). The applied reference standards were IA-R005 (Beet sugar) with a $\delta^{13}C_{V\text{-}PDB}$ value of -26.03 ‰, IA-R001 (wheat flour) with a $\delta^{13}C_{V\text{-}PDB}$ value of -26.43 ‰ and IA-R006 (sugar from cane) with a $\delta^{13}C_{V\text{-}PDB}$ value of -11.64 ‰ The mean standard deviation for $\delta^{13}C$ of IA-R005, IA-R001 and IA-R006 is 0.14 % (n = 10), 0.23 % (n = 10) and 0.53 % (n = 10), respectively.

3.4. MT index

An index for the variable input of marine versus terrigenous organic matter (MT index) was designed applying a modified version of the method described in Bertrand et al. (2012) and Sepúlveda et al. (2009). In brief, the MT index is calculated by a linear regression between the score of the first axis of a principle component analysis (observation scores F1: 93.06 %; F2: 6.94 %, Tab. S4) and its variables: $\delta^{13}C_{org}$ and the fraction of terrestrial organic carbon (F_{terr}), which is calculated from the N_{org}/C_{org} ratio (Perdue and Koprivnjak, 2007; data in the Tab. S2). To calculate F_{terr}, the lowest and highest N_{org}/C_{org} ratios (0.052; Site 314, 0.113; Site 502) were used to define the terrestrial and the marine end member, respectively. The resulting equation is MT index = 16.68 - 0.034 * F_{terr} + 0.65 * $\delta^{13}C_{org}$ and positive (negative) MT index values indicate higher (lower) marine OM input. The MT index does not consider lacustrine components. We ultimately apply the MT index on the surface set of samples as a baseline for an improved evaluation of changes in marine versus terrigenous OM supply into the fjord on longer time scales. By using the end members for

N_{org}/C_{org} given in this paper, the MT index can be calculated not only for any surface sediment samples but also for long sediment cores retrieved in the Trondheimsfjord for follow up studies. Instead of interpreting relative variation of raw $\delta^{13}C_{org}$ and N_{org}/C_{org} data, the MT index combines both parameters and provides the possibility to compare past changes of marine versus terrigenous OM with the modern distribution of the OM in the Trondheimsfjord.

3.5 Bulk mineral assemblage analyses

Bulk mineral assemblages were measured via X-ray diffraction (XRD) using a Philips X'Pert Pro MD, Cu-radiation (k(alpha) 1.541, 45 kV, 40 mA) and X'Celerator detector system at the Central Laboratory for Crystallography and Applied Material Sciences (ZEKAM), University of Bremen, Germany. Samples were prepared by means of the Philips/Panalytical back loading system and a fixed divergence slit (1/4°2θ) with a detection angle from 3°-85° 2θ and a step size of 0.0168° 2θ was used. The calculated time was 100 s per step. Quantification of the mineral content was carried out with Quantitative Phase-Analysis with X-ray Powder Diffraction (QUAX) (details are given in Vogt et al., 2002). Results and error (rel. %) are shown in Tab. S3.

3.6 Elemental composition of terrestrial material

In order to compare our results with geochemical studies from the terrestrial area surrounding the Trondheimsfjord, we used two data sets including overbanked sediments and bedrock analyses. The bedrock analysis reflects the chemical composition of geological units. Overbanked sediments (also called alluvial soil, levée or floodplain sediments) accumulate during active widespread erosion related to flooding episodes. They are

considered to represent the average lithological input of a whole catchment area upstream from the sampling site (Ottesen et al., 1989).

Ottesen et al. (2000) reported the natural chemical composition of 38 overbanked sediments samples (< 63 μm) collected across Trondheimsfjord drainage area using X-ray fluorescence analyses at the Geological Survey of Sweden.

Finally, 183 bedrock samples were available from the Trondheimsfjord drainage area as part of the regional mapping program at the NGU. The chemical composition of these samples (Tab. S5) were determined on a Philips PW 1480 X-ray spectrometer (XRF) at the Geological Survey of Norway (NGU). The locations of the samples are plotted in the simplified geological map (Fig. 2).

4. Results and Discussion

4.1. Mineral assemblages and grain size

The mineral assemblages of surface sediments from Trondheimsfjord are characterized, generally, by high concentrations of metamorphic minerals consistent with the local geology (Fig. 2 and section 2.1), indicating the material to be of local origin and freshly weathered. The XRD analyses reveal that, on average, more than one third of the sediment is composed of phyllosilicates (34.2 %), followed by quartz (22 %), plagioclase (19.5 %) and illite+mica (18.2 %). Calcite (2.2 %), aragonite (0.4 %) and other carbonates (1.9 %) are, on average, only poorly represented in Trondheimsfjord sediments (Tab. S3).

Previously, Howe et al. (2010) reported that the distribution of sediments within fjords depends on its bathymetry and the hydrographic regime. In the Trondheimsfjord, mineral

assemblages and grain sizes were, in some cases, highly variable, even over relatively short distances, most likely due to the inflow of rivers and rapid changes in water depth; however, no correlation between water depth and any grain size fraction was found ($r^2 = < 0.09$), although a general pattern of increasing grain size from the inner fjord to the fjord mouth could be observed (Fig. 3).

This observation is consistent with the XRD analyses, which also shows an increasing trend in the amount of quartz (17.3 % to 26.1 %) and a decrease in illite/mica (21.5 % to 7.9 %) and phyllosilicates (42.9 % to 16.3 %) (Tab. S3), on going from the inside to the outer parts of the fjord. We suggest that the increase in grain size is mainly related to current speed, especially due to tidal currents. This is particularly well illustrated at the fjord entrance where the in- and outflowing (tidal) currents are forced through the narrow passage and above the Agdenes sill (Fig. 1). The high mean current velocity (0.2 m/s) results in sediment winnowing (Jacobson, 1983) and thus enrichment in the coarser grain fractions. Since the velocity of the tidal current decreases towards the inner fjord (less water has to be transported), the proportion of fine grained material increases in that area.

4.2. Sources of organic matter

In order to estimate the relative contributions of marine versus terrigenous organic matter (OM) to the surface sediments in Trondheimsfjord, we examined the stable isotope composition of organic carbon ($\delta^{13}C_{org}$) and the ratio of total organic carbon (C_{org}) to total organic nitrogen (N_{org}) (Fig. 4). In contrast to C_{org} only, these parameters are independent of changes in sedimentation rate and their differences for marine and terrigenous OM have been investigated and utilised extensively in previous studies (Goñi et al., 1997; Stein and MacDonald, 2004 and references therein; Karageorgis et al., 2005; Winkelmann and Knies,

2005; Perdue and Koprivnjak, 2007; Knies and Martinez, 2009; Sepúlveda et al., 2009; Knudson et al., 2011; Sepúlveda et al., 2011; Bertrand et al., 2012). Terrigenous OM is relatively depleted in nitrogen, and characterized by C_{org}/N_{org} ratios >15, compared to marine OM with a significantly lower C/N signature (e.g. Bordovskiy, 1965; Stein and MacDonald, 2004; Rullkötter, 2006). The stable isotope composition ($\delta^{13}C_{org}$) of OM reflects the isotope composition of the different carbon sources and the fractionation of ^{12}C and ^{13}C during photosynthesis (e.g. Hayes, 1993). In general, the carbon source for marine organisms is enriched in ^{13}C compared to atmospheric CO_2 (carbon source for land plants) and the fractionation factor for plants using the C_3 pathway for carbon fixation, typical for high latitude regions (Collins and Jones, 1986; Still et al., 2003), is also larger than for marine organisms (O'Leary, 1981; Schubert and Calvert, 2001; Rullkötter, 2006) which results in higher $\delta^{13}C_{org}$ values for marine OM compared to terrigenous OM (e.g. Schubert and Calvert, 2001).

The C_{org}/N_{org} ratios of the surface sediment samples from Trondheimsfjord show an increase from the entrance of the fjord (e.g. C_{org}/N_{org} = 8.8; Site 502) towards the inner fjord (e.g. C_{org}/N_{org} = 14.3; Site 201) (Fig. 4) with highest values occurring in the samples closest to river inlets (e.g. C_{org}/N_{org} = 19.1; Site 314). In contrast to the C_{org}/N_{org} ratios the $\delta^{13}C_{org}$ values in the surface sediments show the opposite trend (Fig. 4), decreasing from the outside towards the inside of the fjord. Highest (-21.2 ‰; Site 502) and lowest values (-26 ‰; Site 324) values were found for sites corresponding to the entrance of the fjord and river deltas, respectively. Furthermore, as expected from the spatial distribution $\delta^{13}C_{org}$ and N_{org}/C_{org} correlates well (r^2 = 0.74, Fig. 5).

The systematic relationship between $\delta^{13}C_{org}$ signatures and the N_{org}/C_{org} ratio have been used to establish a two end member mixing model (for mathematical reasons we use the N_{org}/C_{org} ratio here, seePerdue and Koprivnjak (2007)). All data show that the composition of sedimentary organic matter in surface sediments is consistent with mixing of marine and terrigenous C3-photosynthetic organic matter. As discussed previously, the admixture of C4 plant types is insignificant in the study region (Collins and Jones, 1986; Still et al., 2003) and does not influence the binary system of the two end members (terrestrial vegetation/soil and marine organic matter). Furthermore, the regression of N_{org}/C_{org} vs $\delta^{13}C_{org}$ (Fig. 5) for the studied sample set indicates that the proposed N_{org}/C_{org} end member values (0.052; 0,113) corroborate typical $\delta^{13}C_{org}$ based end members for terrestrial (-27 ‰) and marine OM (-21 ‰ - -20 ‰) in the study region (Knies, 2005; Winkelmann and Knies, 2005; Knies and Martinez, 2009).

The resulting MT index (Fig. 6), which builds on the overall good regression of N_{org}/C_{org} vs. $\delta^{13}C_{org}$ (Fig. 5), trace the change from more terrigenous OM in the inner fjord towards higher relative abundances of marine OM in the sediments towards the entrance. Thus, the MT index is sensitive for evaluating the origin of the OM (Jasper and Gagosian, 1990) and this is demonstrated convincingly for the locations studied here (Fig. 6).

Bøe et al. (2003) reported sedimentation rates between 0.4 and 2.5 mm/year over the past 6000 years in the Seaward and Middle fjord basin based on eleven sediment cores. Assuming these sedimentation rates our surface sediments contain a record of 25 to 4 years. Most of our samples, however, were very fluffy due to a high content of water and furthermore ^{210}Pb-dating results of four multicores from different basins (Entrance, Seaward, Middle fjord) reveal sedimentation rates of 5-7 mm/year for the past 60 years

(Milzer et al., 2013b). We assume therefore, that our results mirror modern environmental conditions.

The reliability of the MT index as a proxy for the origin of the OM can be demonstrated further by comparison with the modern primary production in the Trondheimsfjord. Volent et al. (2011) studied the spatial and temporal evolution of phytoplankton blooms in the Trondheimsfjord from March to October 2004 by combining the analysis of water samples, and data from a ship-mounted automatic flow through sensor system, Ferrybox (measuring Chlorophyll a and turbidity) with red, green, blue (RGB) colour satellite images and remotely sensed total suspended matter (TSM) from the MERIS instrument aboard the satellite ENVISAT (ENVIronmental SATellite, European Space Agency). Volent et al. (2011) reported that high turbidity (cloudy water in the RGB images and high TSM concentrations) was not related to suspended minerals of nonbiological origin, but was caused by loose coccoliths (calcium carbonate plates of coccolithophores) as well as by large cells with high pigment content. Thus, the measured turbidity was interpreted as reflecting primary production in the fjord. Even though the images from Volent et al. (2011) only reveal a snapshot of the annual primary production in the Trondheimsfjord, a strong visual correlation with our MT index data is clear (Fig. 6). According to the MT index values, the turbidity (phytoplankton) concentration is highest at the fjord entrance and in the centre part of the Seaward basin and decreases towards the river deltas and the inner part of the fjord. In addition, the distribution of phytoplankton in Trondheimsfjord is related to river runoff and surface water circulation (Sakshaug and Myklestad, 1973; Volent et al., 2011) and is most obvious in the channel behind the Tautra sill. In this region, we find high MT index values on the south side compared to the north side. Satellite images (Volent et al., 2011) reveal that turbid,

coccolith-rich, inward flowing surface water from the Seaward basin crosses the Tautra sill on the southern side whereas the outward flowing surface water on the north side is clearer. The distribution of phytoplankton, therefore, potentially helps to explain the variations in MT indices over short distances near the Tautra sill and illustrates the important role of the inflow pattern of oceanic water for the distribution of marine OM versus terrigenous OM in Trondheimsfjord sediments. Finally, the distribution of $\delta^{13}C$ in benthic foraminifera from the Trondheimsfjord is very similar to the MT index. Milzer et al (2013a) found a general increasing trend of $\delta^{13}C$ in benthic foraminifera from the inner Trondheimsfjord towards the open ocean with lowest values close to river deltas. In accordance to our findings, Milzer et al. (2013a) assume terrigenous derived C_{org} to be responsible for lower $\delta^{13}C$ values at river deltas and the inner part of the fjord marine derived C_{org} for the increasing $\delta^{13}C$ values towards the fjord entrance.

Only two samples sites (Site 329, south of the Agdenes sill and Site 214, northeast of the Tautra sill) fail to fit into the observed pattern (Fig. 6). Analysis from the deepest part at the entrance of the fjord (Site 329; water depth 605 m; MT index = -0.75) indicates a more terrestrial source of the OM compared to the surrounding sample sites. Site 329 is close to a disposal place for ships and explosives and, therefore, the OM could be anthropogenically influenced; although, we do not find any other indication for contamination in this area from the inorganic analyses and currently have no firm explanation for this discrepancy. In contrast, data from Site 214 indicates a more marine source of the OM compared to the surrounding stations, with a MT index value of 1.54. This area is a well-known fishing ground (O. Longva, pers. comm. 2012), as supported by numerous fish bones in the sample and the hinterland region is used intensively for agriculture. Thus, the OM is probably altered by

marine organic waste and nitrogen-rich fertilizer. This is supported by a $\delta^{13}C_{org}$ value (-22.35 ‰) which is in line with the values of the surrounding samples (Fig. 4).

To summarise the organic geochemical analyses, the MT Index appears to represent an excellent tool for distinguishing, semi-quantitatively, between marine and terrigenous OM for the majority of the surface sediments from the fjord. The clear proximal to distal trend of the MT index is in agreement with previous investigations of fjords in northern Patagonia. The terrestrial index based on $\delta^{13}C_{org}$ and salinity (Bertrand et al., 2012), for example, shows a decreasing trend from the fjord inner part towards the open ocean. Similarly, Sepúlveda et al. (2011) found a strong gradient (84 % difference) of organic carbon sources between open ocean areas and those located towards inner fjords and/or river outlets using a combination of C_{org}/N_{tot}, $\delta^{13}C_{org}$ and $\delta^{15}N$ data. Collectively, these findings reveal that changes in the terrigenous vs. marine OM input in fjords are mostly controlled by two opposing and fundamental processes: (1) the inflow of freshwater transporting terrigenous OM and (2) the inflow of oceanic waters supporting marine organisms e.g. through higher salinities. In the Trondheimsfjord, the freshwater supply is controlled by continental precipitation and temperature (snowmelt), while the inflow of Atlantic water is mainly controlled by the strength of tides, bathymetry, the amount of river run-off, as well as the strength of the NAC flowing along the Norwegian coast. On a smaller scale, the fjord surface circulation may also play an important role in the distribution of marine versus terrigenous OM in fjord sediments, as illustrated by the variations in the MT index in the Middle fjord basin close to the Tautra sill (Fig. 6). Since the inflow of Atlantic water and precipitation pattern in central Norway are linked via NAO and NAC to large-scale climate systems (Hald et al., 2011; Pinto and Raible, 2012), well-constrained (temporally) MT index records from the Trondheimsfjord

may be used as a proxy-based method for further Holocene climate change studies in the future.

4.3. Bulk inorganic sediment composition

4.3.1. Marine source

Ca and $CaCO_3$ in Trondheimsfjord sediments are strongly correlated (r^2=0.97, n = 60) and corroborate the spatial pattern of the MT index data (Fig.7 and 8). Both parameter (Ca and $CaCO_3$) show a clear proximal to distal trend in the Trondheimsfjord sediments with highest values at the entrance and lowest values in the inner part of the fjord and river deltas (Fig 7 and 8). However, the overall regression of the MT index vs. Ca and $CaCO_3$, respectively, is relatively poor (both r^2 = 0.3, n = 60). One possible explanation for this discrepancy lies in the extremely high Ca and $CaCO_3$ concentrations for five sampling locations (mean Ca = 7.9 %; mean $CaCO_3$ = 18.3 %) compared to the mean value for the entire dataset (Ca = 2.9 %; $CaCO_3$ = 4.6 %; n=60). Samples from these locations are the only samples where aragonite (1.6 - 6.0 %) was present (Tab. S3). This indicates that eroded remnants of the deep water coral *Lophelia pertusa,* which grows at the entrance of the fjord and on the Tautra sill (Mortensen et al., 2001 and reference therein) are the source for the carbonate enrichments. By excluding these five samples (Sites 500, 501, 502, 329 & 217) the overall regression between the MT index increases significantly for $CaCO_3$ (r^2 = 0.6, n = 60) but only slightly for Ca (r^2 = 0.4, n = 60). Our findings show that the latter is likely explained by the dilution of marine produced carbonates with terrigenous Ca bearing minerals (e.g. amphibole). Indeed, alluvial soil samples show a fairly homogenous distribution of Ca in the catchment area of the fjord (Fig. 7), with mean Ca concentration of 2.5 % (Ottesen et al.

2000). Moreover, samples recovered along the shore and in river deltas with a negative MT index show no relation between Ca and the MT index (Fig 9). $CaCO_3$ is only slightly related to the negative MT index values ($r^2 = 0.2$) and also Ca and $CaCO_3$ show no connection in samples with a negative MT index ($r^2 = 0.04$, n= 29). These findings express the influence of a terrestrial Ca source on biogenic components in samples close to the shore and in river deltas.

Samples with MT index values > -0.7 (Fig. 9) reveal a good correlation of Ca and the MT index ($r^2 = 0.57$, n =43). The regression becomes even stronger ($r^2 = 0.77$, n = 39) by excluding the samples enriched in aragonite from eroded deep water corals (Fig. 9). Also the regression between $CaCO_3$ and Ca in samples with MT index values > -0.7 increases significantly, $r^2 = 0.98$ (n = 43). The strong correlation between Ca and $CaCO_3$ points to biogenic calcite as the main Ca source in samples with positive MT index values. This assumption is further supported by clear negative correlations (r = -0.6 to -0.8) of Ca and $CaCO_3$ with any terrigenous element (e.g. Al, Fe, Ti, and Zr).

As a result, variations in the concentrations of Ca and $CaCO_3$ in samples with positive MT index values can be treated as a proxy for carbonate marine productivity and may serve as an indicator for the variable inflow of North Atlantic water masses versus river discharge.

4.3.2. Terrestrial sources

In the following section, we discuss the changes in the geochemical composition of the terrigenous fraction in the surface sediments and identify possible land sources by studying the behaviour of Al-based ratios. From the 35 analysed elements, we focus on the elements Ni and K as their spatial distribution can be directly related to the available bedrock and

alluvial soil measurements in the hinterland. The variation in grain size and mineral assemblage may have contributed to some trace element variability (e.g. Loring, 1990 and references therein). Elemental ratios are insensitive to dilution effects and by using a normaliser incorporating mainly in a single grain size fraction the grain size effect can be minimized. Al is a conservative element, showing a strong correlation ($r^2 = 0.8$) with grain size fraction < 63 µm in our study area and Bertrand et al. (2012) found that Al is relatively insensitive to changes in the nature of sediment sources, catchment size, and hydrodynamic sorting in fjords of northern Patagonia.

4.3.2.1. Proxies for terrestrial sediment supply from the southern hinterland

Ni/Al ratios show highest values close to the river deltas of Orkla, Gaula and Nidelva in the southwest and decrease towards the inner and outer part of the Trondheimsfjord (Fig. 10). Alluvial soil which are assumed to represent the overall geochemical signature of the catchment areas (Ottesen et al., 1989) show elevated Ni values in the southern hinterland (Fig. 10; Ottesen et al., 2000). Ottesen et al. (2000) also found that Ni in alluvial soil correlated well with Cr and Mg, suggesting that the main sources for Ni were iron-magnesium minerals e.g. olivine, amphibole and pyroxene. Consistent with the observations of Ottesen et al. (2000), Ni correlates best with Mg ($r^2 = 0.9$) and Cr ($r^2 = 0.9$) in the fjord surface sediments, pointing to a distinct Ni source located in the southern hinterland. This conclusion is supported further by the bedrock analyses, that reveals high Ni concentrations in the greenstones and metagreywackes located along the southern side of the fjord (Fig. 10). Other geochemical investigations of urban surface soil from Ottesen and Langedal (2001) and Andersson et al. (2010) exhibit no anthropogenic Ni contamination by the city of Trondheim and attributed elevated Ni concentration by the presence of greenstone

bedrocks. This suggests that the elevated Ni/Al values are natural and related to changes in the terrestrial sediment supply from the southern hinterland. Furthermore, temporal changes in Ni/Al are, thus, likely the result of changes in erosion and runoff in the southern hinterland that, in turn, are controlled by precipitation and temperature variability.

4.3.2.2. Proxies for terrestrial sediment supply from the northern hinterland

A precise association of K to a specific mineral does not exist. Several studies (e.g. Shimmield, 1992; Martinez et al., 1999) reported potassium feldspar ($K[ALSi_3O_8]$) and illite ($(K,H_3O)Al[(OH)_2Si_3AlO_{10}]$) (e.g. Yarincik et al., 2000) as the dominant K source in marine sediments deposited in upwelling regions or restricted basins (Cariaco Basin). In the Trondheimsfjord surface sediments K is not related to the amount of potassium feldspar ($r = -0.44$) and like Al, K correlates well with the clay fraction ($r^2 = 0.8$). As a result, the distribution of K in the Trondheimsfjord sediments is related to the concentration of phyllosilicates ($r^2 = 0.6$), however, K has no affiliation to a specific clay mineral. Best regression was found with illite $r^2 = 0.2$. These findings suggest that the analysed K originates potentially from a mixture of different (clay) minerals and maybe also from K ions adsorbed to clay minerals (Müller, 1977). Additional analyses are necessary to define the specific K source in the Trondheimsfjord sediments. Nevertheless, K/Al values in the surface sediments are highest in inner fjord (Beitstadfjord and Middle fjord) and at the mouth of the Steinkjerelva river (Fig. 11). They decrease continuously towards the fjord entrance suggesting a K source in the northern drainage area of the Trondheimsfjord. The comparison of these findings with geochemical investigations of bedrock and overbanked sediments on land, further confirms this suggestion. Precambrian felsic volcanic rocks related to a tectonic window called *Tømmerås anticline* (see Roberts, 1997 for details) in the north-eastern

hinterland (Fig. 2) show highest K concentration (average > 4 %) in the hinterland bedrock (Fig. 11). Ottesen et al. (2000) found highest K concentration in samples from the *Tømmeråsanticline* region compared to the rest of the fjord catchment area (Fig. 11). Depending on the freshwater discharge, fine grained K-rich material can be transported over large distances above the halocline in the brackish surface layer (Hoskin et al., 1978). As such, we suggest that temporal changes of K/Al are an indicator of the variable supply of sediments from the northern hinterland of the Trondheimsfjord.

To summarise, we show that the inorganic geochemical composition of surface sediment from the Trondheimsfjord reflect regional differences in the geology of the terrestrial source area. Specifically, K is transported from the northern hinterland into the Middle fjord and Ni enters into the Seaward basin from a separate region in the southern hinterland (Fig. 10 and 11). Compared to other Al-based elemental ratios K/Al and Ni/Al show a distinct spatial distribution which is related to the spatial distribution of K und Ni in bedrock and alluvial soil measurements in the hinterland. Thus, the grain size independent distribution of Ni/Al and K/Al in the Trondheimsfjord sedimentary records might be used to investigate past changes in terrestrial input and, thus, reconstruct variable freshwater inflow from separated provinces. Moreover, the distribution of K/Al and Ni/Al are strongly influenced by the fjord bathymetry. The Tautra sill forms the boundary between the Seaward basin and the Middle fjord (Fig. 1) and prevents a free water exchange between these deep basins. By forming a ratio between K (northern province) and Ni (southern province), the strong effect of the sill on circulation and sedimentation in the fjord can be demonstrated (Fig. 12).

It should be noted that in drainage areas with generally lower content of K or Ni, temporal and spatial variations of transport and storage processes, for example due to faster

erosion or variable run-off, could significantly alter the spatial distribution of K/Al and Ni/Al. To exclude this possibility and to finally confirm our findings it is necessary to study the flux rates of production, transport, and discharge of detritus for every drainage basin over longer time periods. Unfortunately, to our knowledge no such data set are available yet and accumulation rates cannot be calculated. However, the strong relation between the spatial variation of elemental concentrations in Trondheimsfjord sediments with their distribution in the drainage area bedrock and overbanked sediments is a strong indicator that hinterland areas with low Ni and low K concentration have a negligible effect on K and Ni concentration in Trondheimsfjord surface sediments. In addition, overbanked sediments are formed along the streams during flood events (Ottesen et al., 1989) and, therefore, they reflect to some extent the river loads. Further investigations of short sediment cores covering the last century will prove the capability of the proxies by comparing K/Al and Ni/Al records to instrumental data such as temperature and precipitation, and thus the erosional capacity of the fjord catchment area.

5. Conclusions and Implications

The geochemical composition of sixty surface sediment samples from the Trondheimsfjord, central Norway, show that the distribution of carbonate and marine C_{org} follow related patterns of primary production within the fjord which are related to the inflow of salty oceanic waters. As such, we propose that a combined marine-terrestrial (MT) index and the carbonate content can be used to recognise past changes in the inflow of North Atlantic derived ocean waters. Furthermore, by analysis of grain size independent elemental ratios such as K/Al, Ni/Al and K/Ni, distinct Ni and K sources in bedrocks and alluvial soil in the southern and northern hinterland, respectively, can be identified in fjord

sediments. In applying this approach for reconstructing past climate in the region, we assume that temporal variations of these ratios are mainly controlled by continental precipitation and the resulting river discharge transporting the material into the fjord. Ultimately, the application of these organic and inorganic proxies on longer time scales will provide a robust reconstruction of past climate changes in central Norway and potentially illuminate both the variability of the North Atlantic Current and the North Atlantic Oscillation since the last deglaciation.

Acknowledgments

We thank the captain Oddvar Longva, and the crew of the RV Seisma for their professional support during our expeditions. Further we would like to express our gratitude to Karine Charlier and Philippe Martinez (EPOC, CNRS/University of Bordeaux 1), Anne Nordtømme, Bjørn Willemoes-Wissing, Clea Elisatbeth Fabian, Melanie Mesli, and Wieslawa Koziel (NGU) for their help with the laboratory work. For their interest, stimulating discussions, and many useful comments we thank our colleagues Simon Belt, Ola Magne Sæther, Rolf Tore Ottesen, Simone Sauer and Anne Liinamaa-Dehls. This work is a contribution to the CASE Initial Training Network funded by the European Community's 7th Framework Programme FP7 2007/2013, Marie-Curie Actions, under Grant Agreement No. 238111.

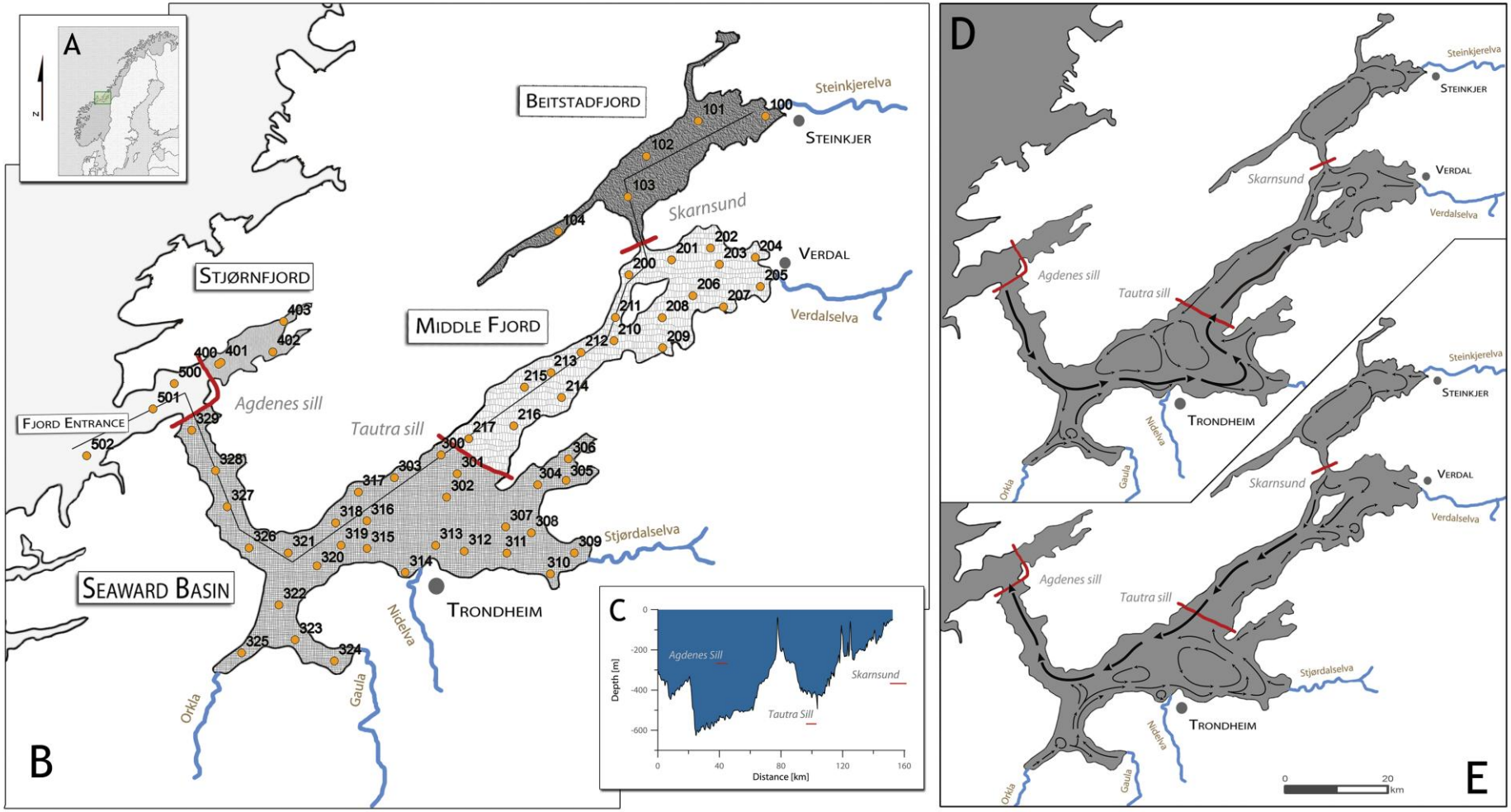

Figure 1: A) Location of the study area. B) Map of the Trondheimsfjord showing the sampling positions (yellow circles. Tab. S1) and the three sills (red lines) dividing the fjord into four main basins as well as the six main rivers entering the fjord from the south/southeast. The thin black line is the path of the bathymetry profile C). Inset: Surface water circulation pattern during high tide phase D) and low tide phase E) (modified after Jacobson, 1983; and Bierach, 1989).

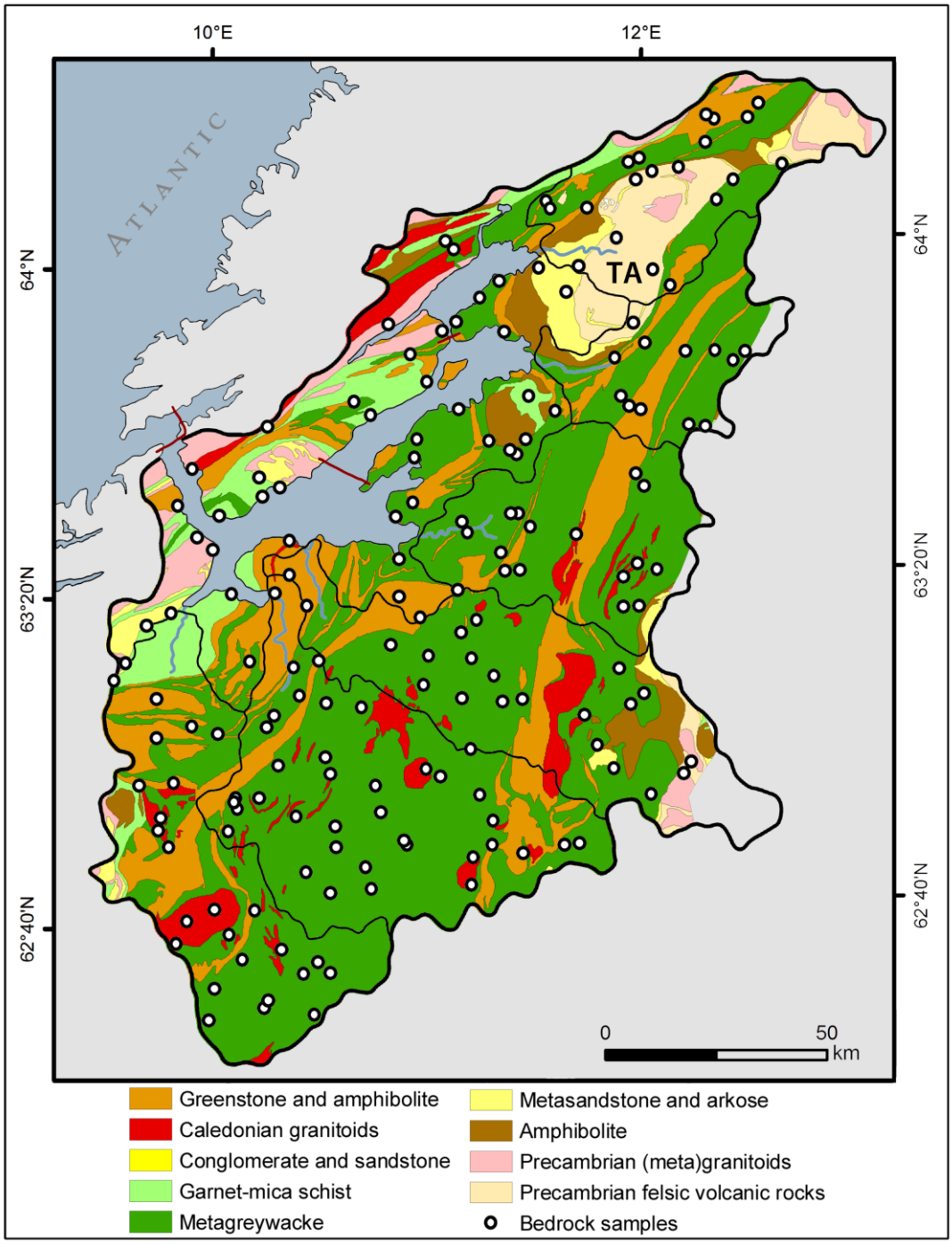

Figure 2: Simplified geological map of the Trondheimsfjord drainage area modified after Koistinen et al. (2001) shows the main lithology and bedrock sampling positions (circles) for the geochemical analyses. *TA* indicates the Tømmerås anticline, see section 2 for details. Coordinates are presented in Tab. S5.

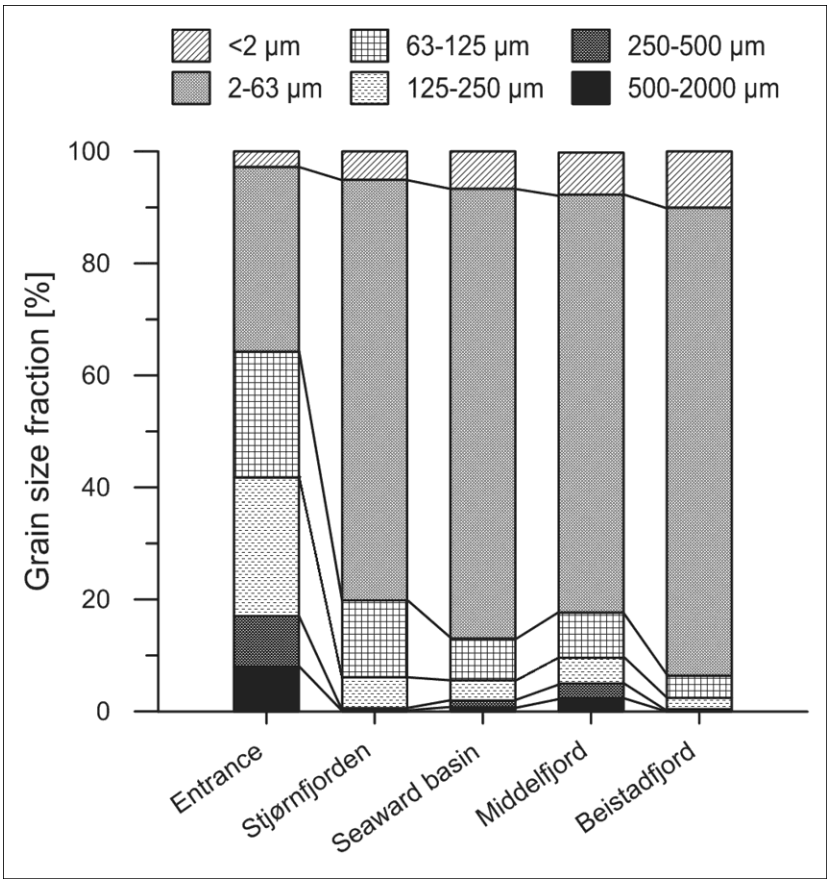

Figure 3: Average grain size distribution for each basin revelling an increase of the fine- and a decrease of the coarse grained fraction from the inside to the outer parts of the Trondheimsfjord. Data are presented in Tab. S3.

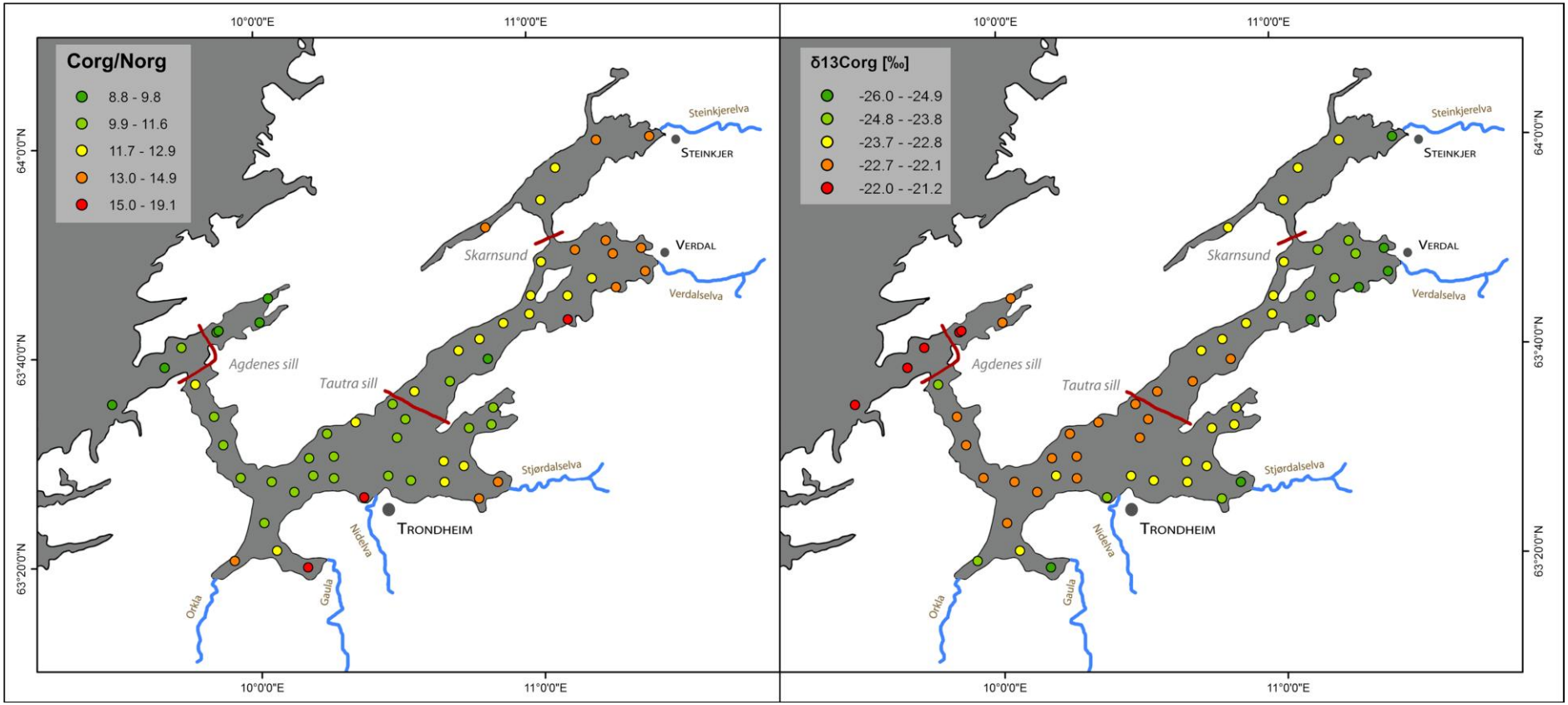

Figure 4: Distribution of C_{org}/N_{org} ratios (left) and $\delta^{13}C_{org}$ (right) of the surface sediments samples. Both parameters show a clear trend from more terrigenous OM at the river deltas and the inner part of the fjord towards more marine OM at the fjord entrance. Data are presented in Tab. S2.

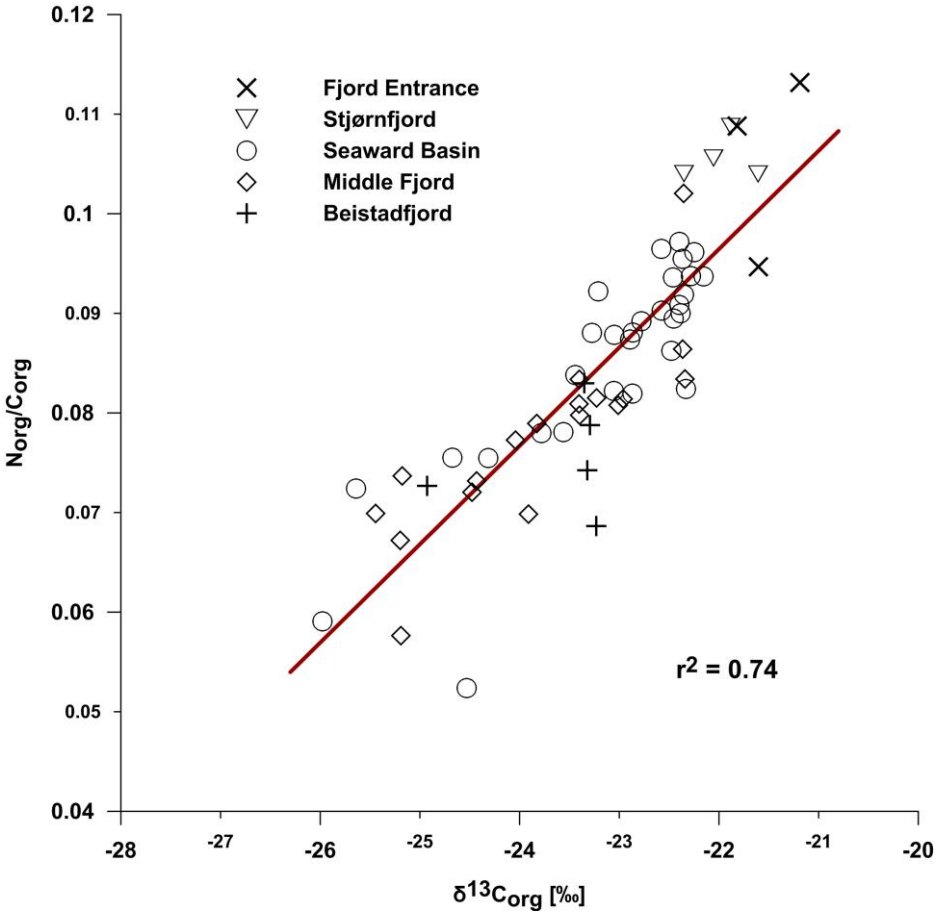

Figure 5: Correlation between N_{org}/C_{org} ratios and $\delta^{13}C_{org}$ in the surface sediments.

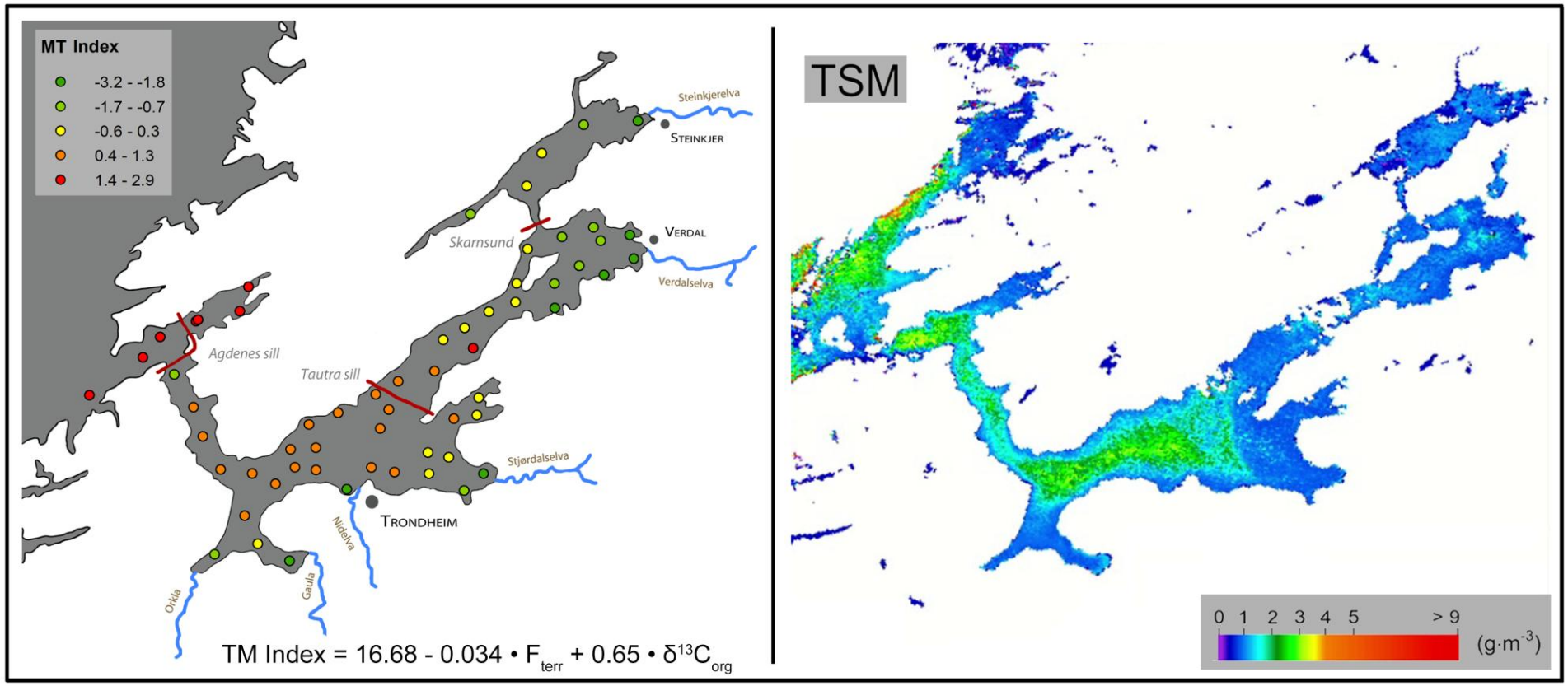

Figure 6: Left: The TM Index combines N_{org}/C_{org} and $\delta^{13}C_{org}$ and can be calculated with F_{terr} in % and $\delta^{13}C_{org}$ in ‰ for any location using the equation displayed at the lower part of the figure. Right: The inside-outside trend of the terrigenous vs. marine OM is in accordance with occurrence of coccoliths and large cells with high pigment content revealed by satellite measurements of the total suspended matter (TSM in g/m^3) recorded on 11.08.2004 and published by Volent et al. (2001).

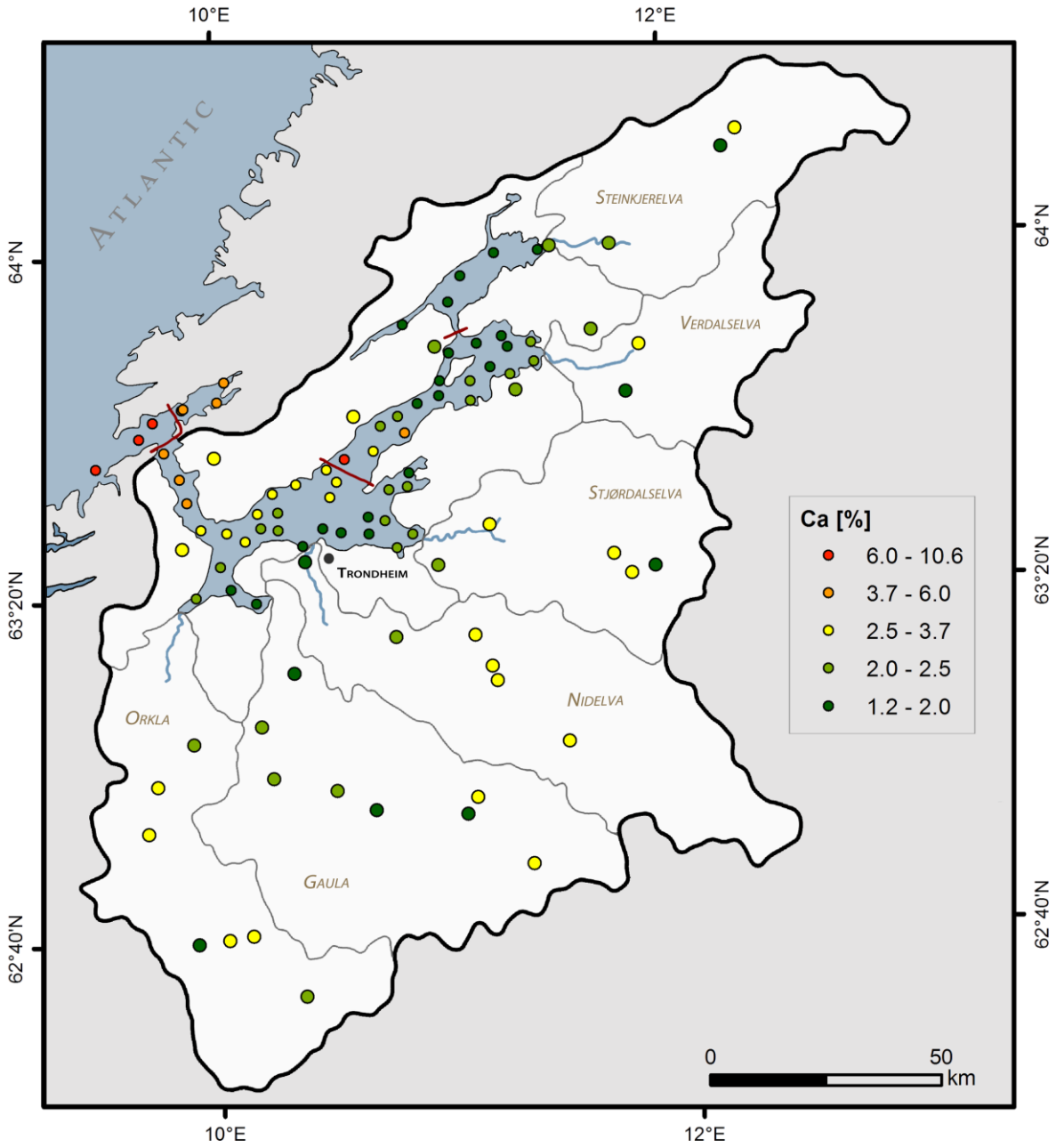

Figure 7: Results of calcium measurements in the surface sediment samples (this study, Tab. S1) and in overbank sediments from Ottesen et al. (2000) in the Trondheimsfjord drainage area. The drainage areas of the six main rivers are indicated by grey lines. The Ca concentrations in the surface sediments show a clear decreasing trend from the entrance towards the fjord inside.

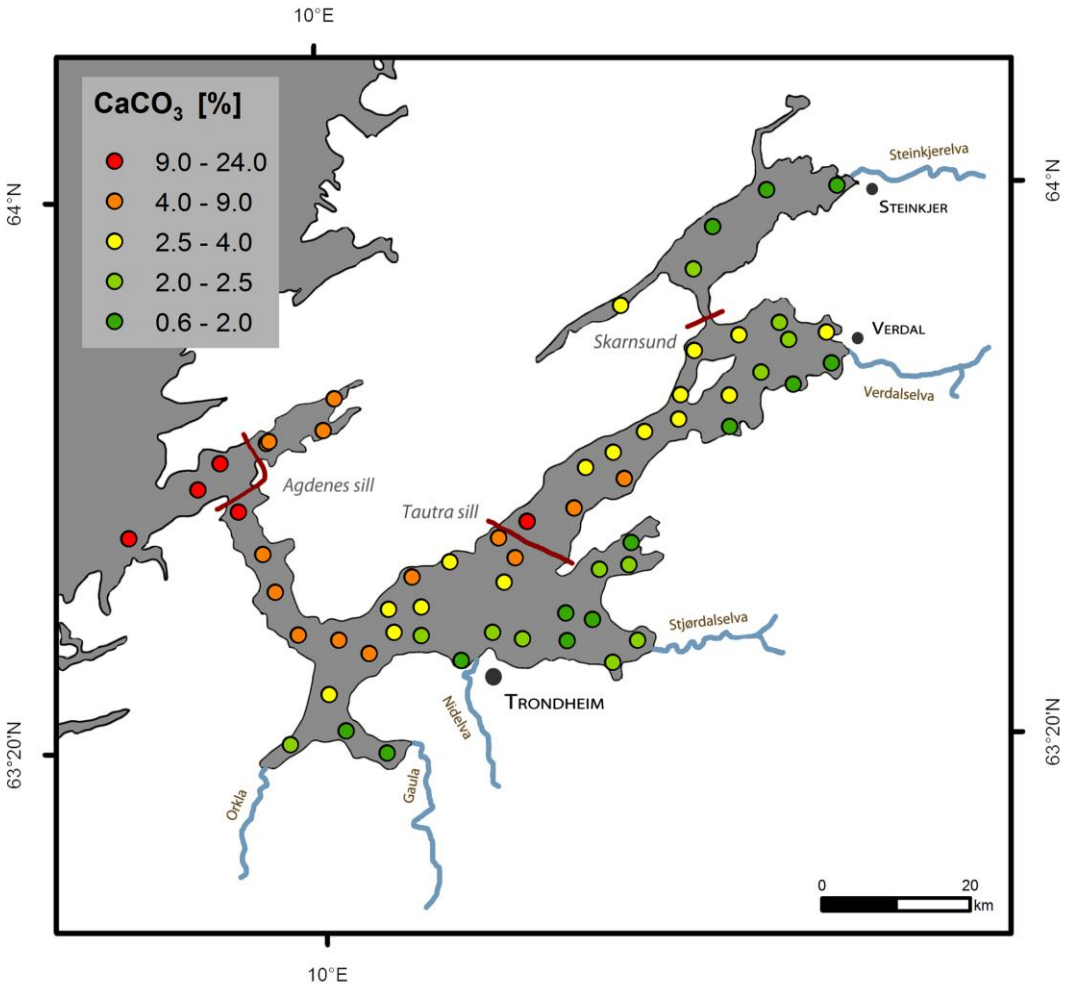

Figure 8: Results of $CaCO_3$ measurements in the surface sediment samples (this study, Tab. S2). The $CaCO_3$ concentrations show a clear decreasing trend from the entrance towards the inner part of the fjord.

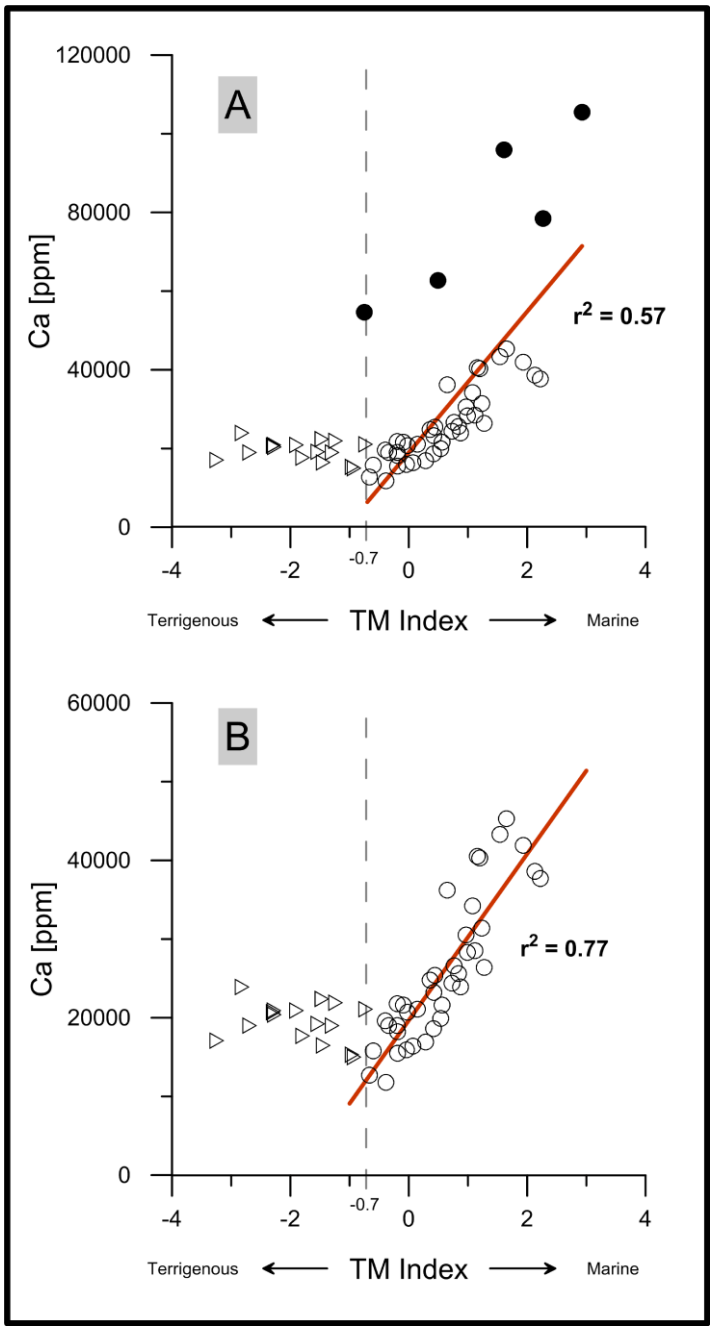

Figure 9: A) Cross correlation between calcium and the MT index for all surface sediments. The red line indicates the regression for samples with a MT index value > -0.7 (circles). Five samples (filled circles) show very high calcium concentration most likely due to abundant coral remains. B) By excluding these samples the relation between calcium and samples with a MT index value > -0.7 (open circles) is much more pronounced indicating large supply of calcium by marine organisms.

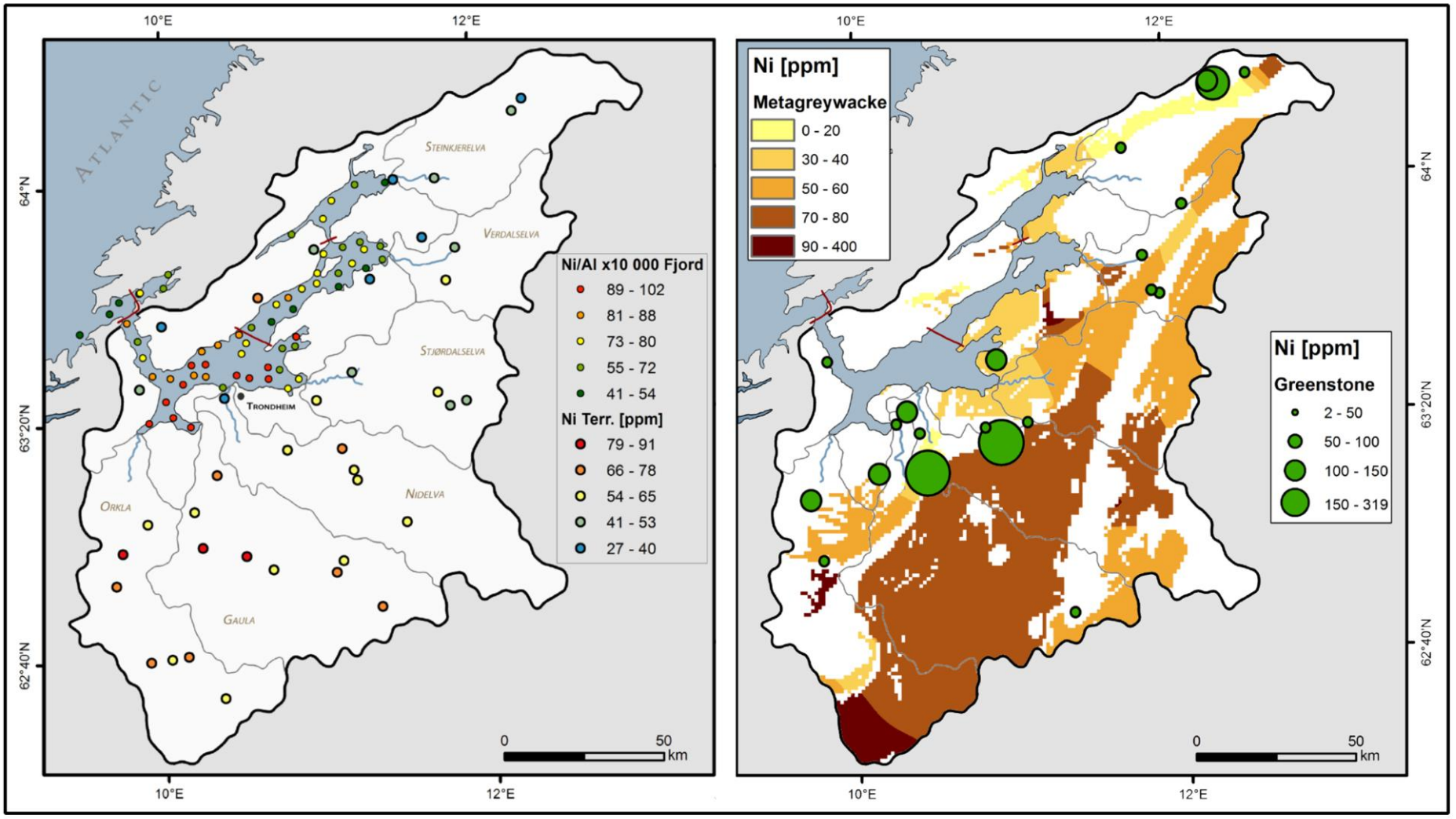

Figure 10: Left: Comparison of the Ni concentration from Ottesen et al. (2000) in the Trondheimsfjord drainage area and Ni/Al in the fjord sediments (this study, Tab. S1). The drainage areas of the six main rivers are indicated by grey lines. Ni/Al in fjord sediments shows highest values close to the river deltas of Orkla, Gaula and Nidelva in the south and decreases towards the inner and outer fjord. This pattern is in accordance with the distribution of Ni in the hinterland. Right: In general our analyses reveal metagreywackes and greenstones to contain highest Ni concentration in the terrestrial bedrock. In accordance with Ottesen et al. (2000) interpolated Ni concentrations within the metagreywackes area (sampling positions are shown in figure 2, data are presented in Tab. S5) and Ni contents in the greenstones samples are highest in the southern hinterland of the fjord.

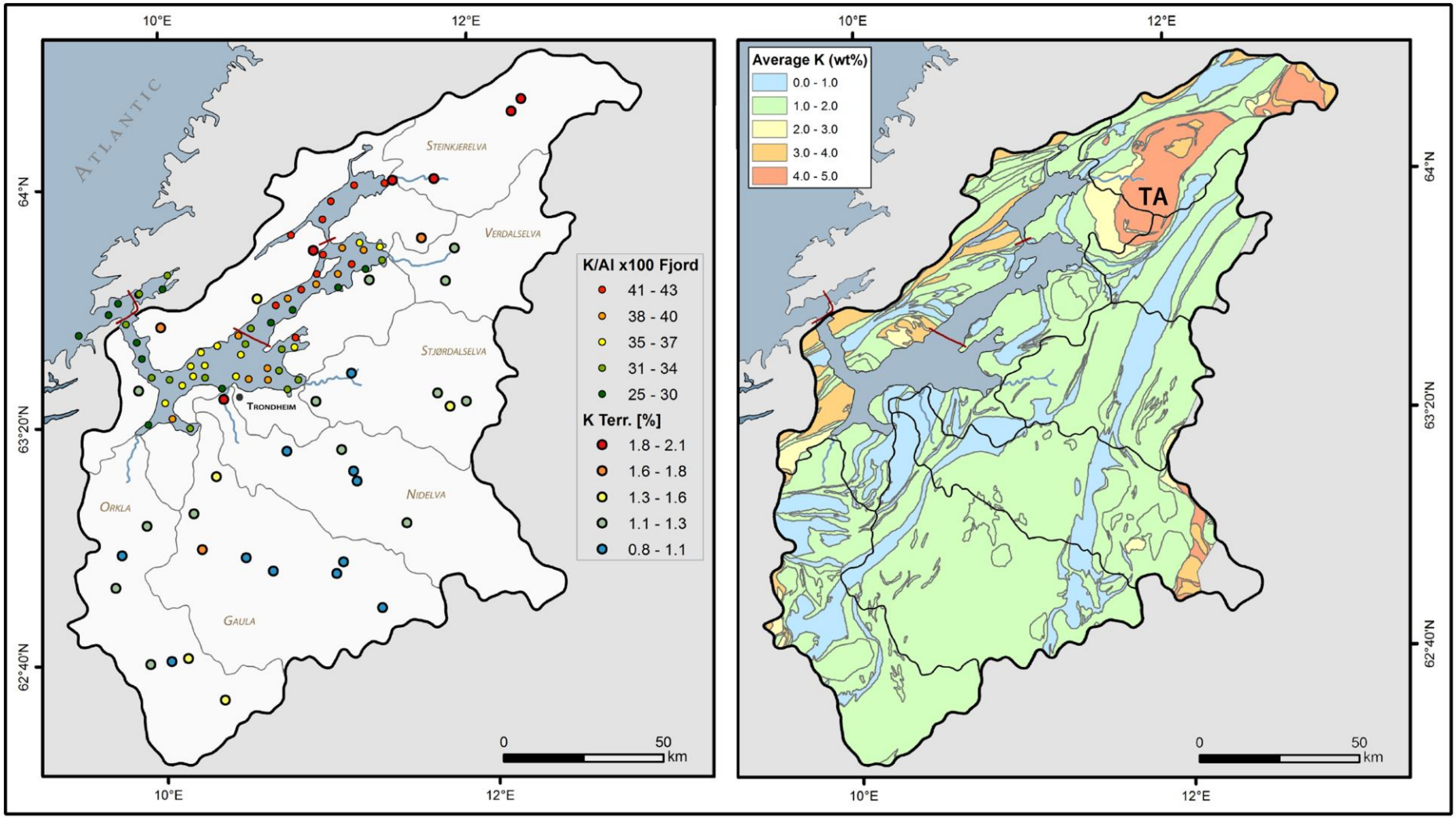

Figure 11: Left: Comparison of the K concentration from Ottesen et al. (2000) in the Trondheimsfjord drainage area and K/Al in the fjord sediments (this study, Tab. S1). The drainage areas of the six main rivers are indicated by grey lines. K/Al in fjord sediments shows highest values close to the Steinkjerelva river delta the in the north and decreases towards the outer fjord. This pattern is in accordance with the distribution of Ni in the hinterland. Right: The chemical data (sampling positions are shown in figure 2, data are presented in Tab. S5) from the various geological units are used to calculate the units' average K concentration. The Tømmerås anticline (TA) in the northern drainage area show highest K concentration (average > 4 %).

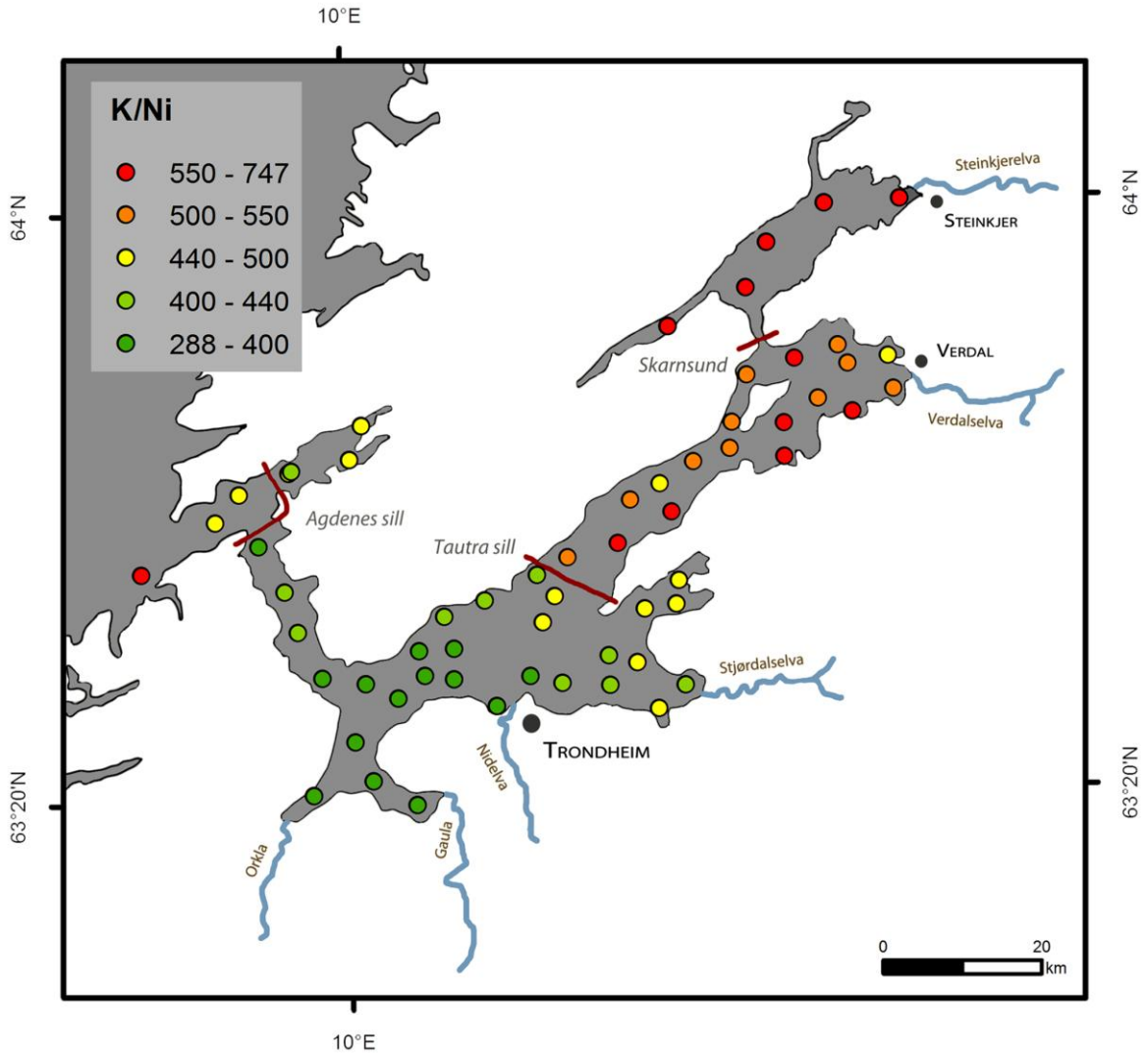

Figure 12: K/Ni in the surface sediments (Tab. S1). The Tautra sill in the middle of the fjord has a strong influence on the water circulation. As a result the K/Ni values are low in the southern and high in the northern part of the fjord.

References

Andersson M., Ottesen R.T. and Langedal M. (2010) Geochemistry of urban surface soils - Monitoring in Trondheim, Norway. *Geoderma* **156**, 112-118.

Bertrand S., Hughen K.A., Sepulveda J. and Pantoja S. (2012) Geochemistry of surface sediments from the fjords of Northern Chilean Patagonia (44-47°S): Spatial variability and implications for paleoclimate reconstructions. *Geochim Cosmochim Ac* **76**, 125-146.

Bordovskiy O.K. (1965) Sources of organic matter in marine basins. *Mar Geol* **3**, 5-31.

Bøe R., Rise L., Blikra L.H., Longva O. and Eide A. (2003) Holocene mass-movement processes in Trondheimsfjorden, Central Norway. *Norw J Geol* **83**, 3-22.

Bøe R., Bugge T., Rise L., Eidnes G., Eide A. and Mauring E. (2004) Erosional channel incision and the origin of large sediment waves in Trondheimsfjorden, central Norway. *Geo-Mar Lett* **24**, 225-240.

Calvert S.E., Pedersen T.F. and Thunell R.C. (1993) Geochemistry of the surface sediments of the Sulu and South China Seas. *Mar Geol* **114**, 207-231.

Cho Y.-G., Lee C.-B. and Choi M.-S. (1999) Geochemistry of surface sediments off the southern and western coasts of Korea. *Mar Geol* **159**, 111-129.

Collins R.P. and Jones M.B. (1986) The influence of climatic factors on the distribution of C4 species in Europe. *Vegetatio* **64**, 121-129.

Goñi M.A., Ruttenberg K.C. and Eglinton T.I. (1997) Sources and contribution of terrigenous organic carbon to surface sediments in the Gulf of Mexico. *Nature* **389**, 275-278.

Govin A., Holzwarth U., Heslop D., Ford Keeling L., Zabel M., Mulitza S., Collins J.A. and Chiessi C.M. (2012) Distribution of major elements in Atlantic surface sediments (36°N–49°S): Imprint of terrigenous input and continental weathering. *Geochem Geophy Geosy* **13**.

Hald M., Salomonsen G.R., Husum K. and Wilson L.J. (2011) A 2000 year record of Atlantic Water temperature variability from the Malangen Fjord, northeastern North Atlantic. *The Holocene*.

Hansen L., L'Heureux J.S. and Longva O. (2011) Turbiditic, clay-rich event beds in fjord-marine deposits caused by landslides in emerging clay deposits - palaeoenvironmental interpretation and role for submarine mass-wasting. *Sedimentology* **58**, 890-915.

Hayes J.M. (1993) Factors controlling 13C contents of sedimentary organic compounds: Principles and evidence. *Mar Geol* **113**, 111-125.

Hirst D.M. (1962) The geochemistry of modern sediments from the Gulf of Paria—II The location and distribution of trace elements. *Geochim Cosmochim Ac* **26**, 1147-1187.

Hoskin C.M., Burrell D.C. and Freitag G.R. (1978) Suspended sediment dynamics in Blue Fjord, western Prince William Sound, Alaska. *Estuarine and Coastal Marine Science* **7**, 1-16.

Howe J.A., Austin W.E.N., Forwick M., Paetzel M., Harland R. and Cage A.G. (2010) Fjord systems and archives: a review. *Geological Society, London, Special Publications* **344**, 5-15.

Inall M.E. and Gillibrand P.A. (2010) The physics of mid-latitude fjords: a review. *Geological Society, London, Special Publications* **344**, 17-33.

Jacobson P. (1983) Physical oceanography of the Trondheimsfjord. *Geophysical & Astrophysical Fluid Dynamics* **26**, 3-26.

Jasper J.P. and Gagosian R.B. (1990) The sources and deposition of organic matter in the Late Quaternary Pigmy Basin, Gulf of Mexico. *Geochim Cosmochim Ac* **54**, 1117-1132.

Karageorgis A.P., Anagnostou C.L. and Kaberi H. (2005) Geochemistry and mineralogy of the NW Aegean Sea surface sediments: implications for river runoff and anthropogenic impact. *Appl Geochem* **20**, 69-88.

Knies J. (2005) Climate-induced changes in sedimentary regimes for organic matter supply on the continental shelf off northern Norway. *Geochim Cosmochim Ac* **69**, 4631-4647.

Knies J., Brookes S. and Schubert C.J. (2007) Re-assessing the nitrogen signal in continental margin sediments: New insights from the high northern latitudes. *Earth Planet Sc Lett* **253**, 471-484.

Knies J. and Martinez P. (2009) Organic matter sedimentation in the western Barents Sea region: Terrestrial and marine contribution based on isotopic composition and organic nitrogen content. *Norw J Geol* **89**, 79-89.

Knudson K.P., Hendy I.L. and Neil H.L. (2011) Re-examining Southern Hemisphere westerly wind behavior: insights from a late Holocene precipitation reconstruction using New Zealand fjord sediments. *Quaternary Sci Rev* **30**, 3124-3138.

Koistinen T., Stephens M.B., Bogatchev V., Nordgulen Ø., Wennerström M. and Korhonen J. (2001) Geological Map of the Fennoscandian Shield, scale: 1: 2,000,000. *Geological Survey of Finland, Norway and Sweden and the North-West Department of Natural Resources of Russia.*

L'Heureux J.S., Hansen L. and Longva O. (2009) Development of the submarine channel in front of the Nidelva River, Trondheimsfjorden, Norway. *Mar Geol* **260**, 30-44.

L'Heureux J.S., Hansen L., Longva O., Emdal A. and Grande L.O. (2010) A multidisciplinary study of submarine landslides at the Nidelva fjord delta, Central Norway - Implications for geohazard assessment. *Norw J Geol* **90**, 1-20.

L'Heureux J.S., Glimsdal S., Longva O., Hansen L. and Harbitz C.B. (2011) The 1888 shoreline landslide and tsunami in Trondheimsfjorden, central Norway. *Mar Geophys Res* **32**, 313-329.

Loring D.H. (1990) Lithium — a new approach for the granulometric normalization of trace metal data. *Mar Chem* **29**, 155-168.

Lyså A., Hansen L., Christensen O., L'Heureux J.S., Longva O., Olsen H.A. and Sveian H. (2008) Landscape evolution and slide processes in a glacioisostatic rebound area; a combined marine and terrestrial approach. *Mar Geol* **248**, 53-73.

Martinez P., Bertrand P., Shimmield G.B., Karen C., Jorissen F.J., Foster J. and Dignan M. (1999) Upwelling intensity and ocean productivity changes off Cape Blanc (northwest Africa) during the last 70,000 years: geochemical and micropalaeontological evidence. *Mar Geol* **158**, 57-74.

Milzer G., Giraudeau J., Faust J., Knies J., Eynaud F. and Rühlemann C. (2013a) Spatial distribution of benthic foraminiferal stable isotopes and dinocyst assemblages in surface sediments of the Trondheimsfjord, central Norway. *Biogeosciences Discuss.* **10**, 5889-5921.

Milzer G., Giraudeau J., Schmidt S., Eynaud F. and Faust J. (2013b) Qualitative and quantitative reconstruction of surface water characteristics and recent hydrographic changes in the Trondheimsfjord, central Norway. *Clim. Past Discuss.* **9**, 4553-4598.

Mortensen P., aring, B. l., Hovland T., Fosså J.H. and Furevik D.M. (2001) Distribution, abundance and size of Lophelia pertusa coral reefs in mid-Norway in relation to seabed characteristics. *Journal of the Marine Biological Association of the United Kingdom* **81**, 581-597.

Mortlock R.A. and Froelich P.N. (1989) A simple method for the rapid determination of biogenic opal in pelagic marine sediments. *Deep Sea Research Part A. Oceanographic Research Papers* **36**, 1415-1426.

Müller P.J. (1977) CN ratios in Pacific deep-sea sediments: Effect of inorganic ammonium and organic nitrogen compounds sorbed by clays. *Geochim Cosmochim Ac* **41**, 765-776.

O'Leary M.H. (1981) Carbon isotope fractionation in plants. *Phytochemistry* **20**, 553-567.

Ottesen R.T., Bogen J., Bølviken B. and Volden T. (1989) Overbank sediment: a representative sample medium for regional geochemical mapping. *Journal of Geochemical Exploration* **32**, 257-277.

Ottesen R.T., Bogen J., Bølviken B., Volden T. and Haugland T. (2000) Geokjemisk atlas for Norge, del 1: Kjemisk sammensetning av flomsedimenter. *Geological survey of Norway (NGU), Norwegian Water Resources and Energy Directorate (NVE)*, Trondheim.

Ottesen R.T. and Langedal M. (2001) Urban geochemistry in Trondheim, Norway. *Norges Geologiske Undersokelse* **438**, 63-69.

Perdue E.M. and Koprivnjak J.F. (2007) Using the C/N ratio to estimate terrigenous inputs of organic matter to aquatic environments. *Estuar Coast Shelf S* **73**, 65-72.

Pinto J.G. and Raible C.C. (2012) Past and recent changes in the North Atlantic oscillation. *Wires Clim Change* **3**, 79-90.

Rise L., Bøe R., Sveian H., Lyså A. and Olsen H.A. (2006) The deglaciation history of Trondheimsfjorden and Trondheimsleia, Central Norway. *Norw J Geol* **86**, 415-434.

Roberts D. (1997) Geochemistry of Palaeoproterozoic porphyritic felsic volcanites from the olden and Tømmerås windows, central Norway. *GFF* **119**, 141-148.

Rullkötter J. (2006) Organic Matter: The Driving Force for Early Diagenesis. in: Schulz, H.D., Zabel, M. (Eds.), Marine Geochmistry, 2 ed. *Springer*, Berlin Heidelberg New York, pp. 125-168.

Sakshaug E. and Myklestad S. (1973) Studies on the phytoplankton ecology of the trondheimsfjord. III. Dynamics of phytoplankton blooms in relation to environmental factors, bioassay experiments and parameters for the physiological state of the populations. *Journal of Experimental Marine Biology and Ecology* **11**, 157-188.

Sakshaug E. and Sneli J.-A. (2000) Trondheimsfjorden. *Tapir Forlag*, Trondheim.

Sargent J.R., Hopkins C.C.E., Seiring J.V. and Youngson A. (1983) Partial characterization of organic material in surface sediments from Balsfjorden, northern Norway, in relation to its origin and nutritional value for sediment-ingesting animals. *Mar Biol* **76**, 87-94.

Schafer C.T., Smith J.N. and Seibert G. (1983) Significance of natural and anthropogenic sediment inputs to the saguenay Fjord, Quebec. *Sediment Geol* **36**, 177-194.

Schubert C.J. and Calvert S.E. (2001) Nitrogen and carbon isotopic composition of marine and terrestrial organic matter in Arctic Ocean sediments:: implications for nutrient utilization and organic matter composition. *Deep Sea Research Part I: Oceanographic Research Papers* **48**, 789-810.

Sepúlveda J., Pantoja S., Hughen K.A., Bertrand S., Figueroa D., León T., Drenzek N.J. and Lange C. (2009) Late Holocene sea-surface temperature and precipitation variability in northern Patagonia, Chile (Jacaf Fjord, 44°S). *Quaternary Res* **72**, 400-409.

Sepúlveda J., Pantoja S. and Hughen K.A. (2011) Sources and distribution of organic matter in northern Patagonia fjords, Chile (~44-47°S): A multi-tracer approach for carbon cycling assessment. *Cont Shelf Res* **31**, 315-329.

Shimmield G.B. (1992) Can sediment geochemistry record changes in coastal upwelling palaeoproductivity? Evidence from northwest Africa and the Arabian Sea. *Geological Society, London, Special Publications* **64**, 29-46.

Stein R. and MacDonald R.W. (2004) The Organic Carbon Cycle in the Arctic Ocean. *Springer*, Berlin Heidelberg.

Still C.J., Berry J.A., Collatz G.J. and DeFries R.S. (2003) Global distribution of C3 and C4 vegetation: Carbon cycle implications. *Global Biogeochem Cy* **17**, 1006.

Syvitski J. and Schafer C.T. (1985) Sedimentology of Arctic Fjords Experiment (SAFE): Project Introduction. *Arctic* **38**, 264-270.

Syvitski J.P.M., Burrell D.C. and Skei J.M. (1987) Fjords: Processes and Products. *Springer-Verlag*, New York.

Syvitski J.P.M. (1989) On the Deposition of Sediment within Glacier-Influenced Fjords - Oceanographic Controls. *Mar Geol* **85**, 301-329.

Vogt C., Lauterjung J. and Fischer R.X. (2002) Investigation of the Clay Fraction (<2µm) of the Clay Minerals Society Reference Clays. *Clays and Clay Minerals* **50**, 388-400.

Volent Z., Johnsen G., Hovland E.K., Folkestad A., Olsen L.M., Tangen K. and Sørensen K. (2011) Improved monitoring of phytoplankton bloom dynamics in a Norwegian fjord by integrating satellite data, pigment analysis, and Ferrybox data with a coastal observation network. *Journal of Applied Remote Sensing* **5**.

Wanner H., Brönnimann S., Casty C., Gyalistras D., Luterbacher J., Schmutz C., Stephenson D. and Xoplaki E. (2001) North Atlantic Oscillation – Concepts And Studies. *Surveys in Geophysics* **22**, 321-381.

Wendelbo P.S. (1970) Hydrografiske forhold i Trondheimsfjorden 1963-66. PhD Thesis, University of Oslo

Winkelmann D. and Knies J. (2005) Recent distribution and accumulation of organic carbon on the continental margin west off Spitsbergen. *Geochem Geophy Geosy* **6**.

Yarincik K.M., Murray R.W. and Peterson L.C. (2000) Climatically sensitive eolian and hemipelagic deposition in the Cariaco Basin, Venezuela, over the past 578,000 years: Results from Al/Ti and K/Al. *Paleoceanography* **15**, 210-228.

Supplementary Paper I

Table S1: Location of sampling stations and list of the presented elements measured by 4 Acid digestion ICP-AES

Sampling station	Latitude (DD)	Longitude (DD)	Water depth (m)	Al (%)	Ca (%)	K (%)	Ni (ppm)	Mg (%)	Cr (ppm)
100	64.0031	11.4382	57	6.68	1.77	2.69	36	1.77	86
101	64.0002	11.2442	157	7.62	1.27	3.2	53	2.29	105
102	63.9580	11.0923	222	7.69	1.18	3.28	59	2.45	110
103	63.9075	11.0352	252	7.73	1.55	3.26	58	2.36	112
104	63.8664	10.8323	128	7.11	1.5	2.92	47	2.05	91
200	63.8090	11.0305	325	7.41	1.96	2.98	57	2.35	113
201	63.8262	11.1542	110	7.27	1.9	2.86	50	2.15	105
202	63.8393	11.2666	82	7.39	1.92	2.73	50	2.19	108
203	63.8183	11.2904	402	7.46	1.65	2.98	56	2.33	114
204	63.8255	11.3938	300	6.68	2.07	2.35	47	2.01	99
205	63.7883	11.4052	81	7.11	2.09	2.37	47	2.05	98
206	63.7801	11.2117	422	7.61	1.53	3.12	57	2.39	112
207	63.7644	11.2976	25	5.7	2.09	1.51	27	1.25	60
208	63.7537	11.1220	421	6.94	2.11	2.7	49	2.13	103
209	63.7157	11.1205	30	5.57	2.39	1.52	23	1.29	65
210	63.7266	10.9822	425	7.65	1.9	3.03	59	2.41	118
211	63.7559	10.9887	416	7.53	1.82	3.12	60	2.48	113
212	63.7129	10.8874	426	7.5	1.9	3.06	60	2.49	114
213	63.6887	10.8005	412	7.78	2.16	3.1	63	2.48	119
214	63.6568	10.8284	72	5.65	4.33	1.39	24	1.27	55
215	63.6711	10.7238	370	7.53	2.07	3.06	60	2.48	114
216	63.6227	10.6901	175	5.88	3.62	1.73	31	1.5	65
217	63.6080	10.5619	212	5.27	6.27	1.63	32	1.41	70
300	63.5885	10.4822	253	7.7	2.83	2.94	68	2.68	124
301	63.5641	10.5268	176	6.55	3.14	2.17	48	1.98	94
302	63.5349	10.4954	165	6.81	2.66	2.4	54	2.12	107
303	63.5610	10.3484	240	6.99	2.54	2.54	58	2.26	118
304	63.5475	10.7542	63	5.97	2.32	1.95	39	1.76	88
305	63.5521	10.8345	62	6.7	2.11	2.31	48	2.05	97
306	63.5791	10.8429	117	7.65	1.69	3.23	70	2.8	134
307	63.4956	10.6603	173	7.56	1.64	3.03	69	2.7	124
308	63.4872	10.7320	82	6.6	2.18	2.19	46	2.02	98
309	63.4602	10.8520	77	6.86	2.04	2.24	54	2.09	115
310	63.4346	10.7829	58	6.44	2.19	2.17	49	2.02	109
311	63.4624	10.6616	177	7.22	1.59	2.89	67	2.57	139
312	63.4661	10.5415	254	7.27	1.86	2.82	69	2.59	138
313	63.4743	10.4608	316	7.32	1.99	2.72	69	2.48	137
314	63.4411	10.3736	71	5.74	1.9	1.57	40	1.63	99
315	63.4723	10.2674	492	6.15	2.16	2.03	51	1.96	114

Table S1 - continued

Sampling station	Latitude (DD)	Longitude (DD)	Water depth (m)	Al (%)	Ca (%)	K (%)	Ni (ppm)	Mg (%)	Cr (ppm)
315	63.4723	10.2674	492	6.15	2.16	2.03	51	1.96	114
316	63.5072	10.2681	483	7.81	2.39	2.83	72	2.72	147
317	63.5436	10.2457	292	7.57	2.64	2.68	64	2.4	132
318	63.5052	10.1794	500	7.73	2.56	2.82	72	2.65	149
319	63.4771	10.1936	504	7.35	2.48	2.51	65	2.46	137
320	63.4517	10.1248	500	7.43	2.85	2.72	71	2.58	150
321	63.4686	10.0443	512	7.1	3.05	2.34	60	2.29	129
322	63.4029	10.0158	433	7.51	2.44	2.68	72	2.61	146
323	63.3586	10.0596	335	7.24	1.58	2.8	74	2.59	151
324	63.3311	10.1693	170	6.31	1.71	2.04	60	1.95	114
325	63.3432	9.9087	301	6.99	2.24	1.9	66	2.38	150
326	63.4755	9.9337	530	6.98	3.42	2.18	57	2.14	119
327	63.5279	9.8733	546	6.21	4.03	1.83	45	1.86	101
328	63.5736	9.8417	566	6.96	4.05	2.02	48	1.95	107
329	63.6251	9.7759	605	5.95	5.46	1.78	48	1.94	116
400	63.7080	9.8546	225	5.75	4.53	1.68	37	1.62	85
401	63.7101	9.8621	225	6.88	4.19	2.25	53	2.22	112
402	63.7226	10.0101	83	6.53	3.77	1.86	42	1.91	95
403	63.7607	10.0419	94	6.9	3.86	2.13	48	2.04	101
500	63.6841	9.7277	115	4.3	9.59	1.09	22	1.07	50
501	63.6525	9.6666	389	4.94	7.84	1.27	26	1.24	57
502	63.5941	9.4771	350	4.59	10.55	1.25	22	1.08	52
			mean	6.8	2.9	2.4	52.1	2.1	108.1
			s.d.[(a)]	0.8	1.8	0.6	14.1	0.4	25.6
			Analytical uncertainty (rel.%) [(b)]	0.6	0.5	1.4	0.8	0.9	2.2
			Lower detection limit (ppm)	100	100	100	2	100	2

[(a)] s.d. = standard deviation (1 sigma)

[(b)] The analytical uncertainty was calculated as 1 s.d. of repeated analyses of every 20th sample

Table S2: Organic geochemistry and calculated MT index

Sampling station	Latitude (DD)	Longitude (DD)	Water depth (m)	TOC (wt%)	TC (wt%)	N_{inorg} (%)	N_{tot} (%)	$\delta^{13}C_{org}$ (‰)	F_{terr} [(a)] (wt%)	MT Index [(b)]
100	64.0031	11.4382	57	1.52	1.75	0.02	0.13	-24.93	66.62	-1.79
101	64.0002	11.2442	157	1.19	1.36	0.04	0.13	-23.32	64.00	-0.66
102	63.9580	11.0923	222	1.24	1.47	0.04	0.14	-23.29	56.57	-0.39
103	63.9075	11.0352	252	1.07	1.35	0.04	0.13	-23.35	49.67	-0.19
104	63.8664	10.8323	128	1.36	1.67	0.04	0.13	-23.23	73.26	-0.92
200	63.8090	11.0305	325	1.03	1.44	0.04	0.12	-23.40	54.91	-0.40
201	63.8262	11.1542	110	0.94	1.24	0.04	0.10	-23.91	71.28	-1.29
202	63.8393	11.2666	82	0.82	1.12	0.04	0.10	-24.48	67.67	-1.54
203	63.8183	11.2904	402	0.94	1.22	0.04	0.11	-24.43	65.78	-1.44
204	63.8255	11.3938	300	0.92	1.27	0.03	0.09	-25.45	71.16	-2.29
205	63.7883	11.4052	81	0.82	1.02	0.03	0.08	-25.20	75.57	-2.28
206	63.7801	11.2117	422	0.97	1.25	0.04	0.12	-24.04	59.04	-0.96
207	63.7644	11.2976	25	0.78	1.00	0.02	0.07	-25.18	64.94	-1.90
208	63.7537	11.1220	421	0.87	1.18	0.03	0.10	-23.83	56.32	-0.73
209	63.7157	11.1205	30	1.11	1.35	0.01	0.08	-25.19	91.31	-2.81
210	63.7266	10.9822	425	1.03	1.43	0.04	0.13	-23.40	49.01	-0.20
211	63.7559	10.9887	416	1.12	1.50	0.04	0.13	-23.23	52.11	-0.19
212	63.7129	10.8874	426	0.97	1.31	0.04	0.12	-23.40	53.06	-0.34
213	63.6887	10.8005	412	1.10	1.47	0.04	0.13	-23.01	53.28	-0.09
214	63.6568	10.8284	72	0.50	1.32	0.01	0.06	-22.35	18.32	1.54
215	63.6711	10.7238	370	1.10	1.49	0.04	0.12	-22.96	52.24	-0.02
216	63.6227	10.6901	175	0.55	1.19	0.01	0.06	-22.36	44.00	0.65
217	63.6080	10.5619	212	0.35	2.17	0.02	0.04	-22.34	48.96	0.49
300	63.5885	10.4822	253	0.97	1.50	0.03	0.12	-22.46	32.19	0.99
301	63.5641	10.5268	176	0.73	1.27	0.02	0.09	-22.40	26.32	1.24
302	63.5349	10.4954	165	0.75	1.18	0.02	0.09	-22.45	38.98	0.76
303	63.5610	10.3484	240	0.80	1.16	0.02	0.09	-22.33	50.59	0.44
304	63.5475	10.7542	63	0.65	0.94	0.01	0.07	-23.21	34.50	0.43
305	63.5521	10.8345	62	0.84	1.10	0.02	0.09	-23.28	41.35	0.15
306	63.5791	10.8429	117	1.25	1.47	0.03	0.14	-23.05	41.66	0.28
307	63.4956	10.6603	173	0.93	1.12	0.03	0.10	-22.87	51.37	0.07
308	63.4872	10.7320	82	0.74	0.93	0.02	0.08	-23.44	48.29	-0.20
309	63.4602	10.8520	77	1.23	1.50	0.02	0.11	-25.64	67.03	-2.27
310	63.4346	10.7829	58	1.02	1.27	0.02	0.09	-24.31	62.01	-1.24
311	63.4624	10.6616	177	0.90	1.06	0.02	0.10	-23.05	50.94	-0.04
312	63.4661	10.5415	254	0.99	1.28	0.02	0.11	-22.87	41.26	0.42
313	63.4743	10.4608	316	0.97	1.25	0.02	0.11	-22.78	39.42	0.54
314	63.4411	10.3736	71	1.20	1.27	0.01	0.08	-24.53	100.00	-2.69
315	63.4723	10.2674	492	0.85	1.13	0.02	0.09	-22.48	44.33	0.56

Table S2 - continued

Sampling station	Latitude (DD)	Longitude (DD)	Water depth (m)	TOC (wt%)	TC (wt%)	N_{inorg} (%)	N_{tot} (%)	$\delta^{13}C_{org}$ (‰)	F_{terr} [(a)] (wt%)	MT Index [(b)]
316	63.5072	10.2681	483	1.01	1.39	0.02	0.11	-22.40	36.72	0.88
317	63.5436	10.2457	292	0.98	1.47	0.03	0.12	-22.25	28.02	1.27
318	63.5052	10.1794	500	1.13	1.57	0.02	0.13	-22.38	38.11	0.84
319	63.4771	10.1936	504	1.08	1.50	0.02	0.12	-22.89	42.43	0.36
320	63.4517	10.1248	500	1.31	1.86	0.02	0.15	-22.28	31.97	1.12
321	63.4686	10.0443	512	1.20	1.79	0.02	0.13	-22.35	35.03	0.97
322	63.4029	10.0158	433	1.11	1.50	0.02	0.12	-22.57	37.68	0.73
323	63.3586	10.0596	335	1.01	1.23	0.02	0.10	-23.56	57.71	-0.60
324	63.3311	10.1693	170	1.02	1.22	0.01	0.07	-25.98	88.96	-3.25
325	63.3432	9.9087	301	1.31	1.56	0.02	0.12	-24.67	61.94	-1.47
326	63.4755	9.9337	530	1.34	2.05	0.02	0.15	-22.58	27.45	1.08
327	63.5279	9.8733	546	0.95	1.73	0.02	0.10	-22.15	32.04	1.20
328	63.5736	9.8417	566	1.19	1.99	0.02	0.13	-22.36	29.12	1.16
329	63.6251	9.7759	605	1.04	2.51	0.02	0.10	-23.78	57.88	-0.75
400	63.7080	9.8546	225	1.19	2.17	0.01	0.14	-21.61	15.13	1.65
401	63.7101	9.8621	225	1.48	2.47	0.02	0.18	-21.88	7.30	1.93
402	63.7226	10.0101	83	1.75	2.49	0.01	0.20	-22.05	12.53	2.23
403	63.7607	10.0419	94	1.87	2.68	0.02	0.21	-22.35	15.09	2.13
500	63.6841	9.7277	115	0.54	3.24	0.01	0.06	-21.60	30.40	1.61
501	63.6525	9.6666	389	0.80	2.91	0.01	0.10	-21.82	7.21	2.27
502	63.5941	9.4771	350	0.71	3.59	0.01	0.09	-21.19	0.00	2.93
			mean	1.0	1.4	0.02	0.11	-23.0	49.0	0.11
			s.d. [(c)]	0.3	0.6	0.01	0.03	1.1	20.7	1.38

[(a)] F_{terr} = fraction of terrestrial organic carbon (Fterr), which is calculated from the Norg/Corg ratio

[(b)] MT Index = index for the variable input of terrigenous versus marine organic matter

[(c)] s.d. = standard deviaton (1 sigma)

Table S3: Mineralogical and sedimentological data

Sampling station	Latitude	Longitude	Water depth	< 2 µm	2-63 µm	63-125 µm	125-250 µm	250-500 µm	500-2000 µm	Calcite	Aragonite	Sum Illit + Mica	Sum Phyllosilicates	Quartz	Plagioclase	K-feldspar
	(DD)	(DD)	(m)	(%)	(%)	(%)	(%)	(%)	(%)	(%)	(%)	(%)	(%)	(%)	(%)	(%)
100	64.0031	11.4382	57	4.9	83.9	5.6	3.9	1.3	0.4	0.5	0.0	15.6	28.3	24.9	28.6	3.5
101	64.0002	11.2442	157	11.5	87.3	1.2	0.0	0.0	0.0	0.4	0.0	14.3	39.0	16.1	18.2	4.0
102	63.9580	11.0923	222	13.1	85.7	1.2	0.0	0.0	0.0	0.3	0.0	23.5	46.9	15.1	18.5	2.9
103	63.9075	11.0352	252	11.2	80.8	4.4	3.5	0.1	0.0	0.5	0.0	31.1	56.6	12.6	18.3	1.4
104	63.8664	10.8323	128	9.5	80.2	7.3	2.9	0.1	0.0	0.4	0.0	22.9	43.6	17.9	22.2	2.9
200	63.8090	11.0305	325	10.7	86.6	2.7	0.0	0.0	0.0	0.7	0.0	13.8	43.4	15.9	16.1	2.1
201	63.8262	11.1542	110	8.3	88.7	3.0	0.0	0.0	0.0	0.6	0.0	24.0	42.6	18.6	18.2	2.2
202	63.8393	11.2666	82	5.9	90.8	3.4	0.0	0.0	0.0	0.5	0.0	23.9	53.1	18.7	15.8	2.1
203	63.8183	11.2904	402	9.6	84.7	3.7	2.0	0.0	0.0	0.4	0.0	34.0	45.1	15.7	16.0	2.4
204	63.8255	11.3938	300	5.9	83.0	8.8	2.3	0.0	0.0	0.8	0.0	21.1	39.0	21.9	21.1	2.6
205	63.7883	11.4052	81	5.0	86.5	6.4	2.1	0.0	0.0	0.4	0.0	20.8	36.7	25.3	22.3	2.2
206	63.7801	11.2117	422	10.0	87.8	2.2	0.0	0.0	0.0	0.5	0.0	33.1	47.2	12.9	17.5	2.1
207	63.7644	11.2976	25	2.6	44.9	13.3	15.9	14.9	8.4	1.3	0.0	19.7	34.7	31.8	20.3	1.8
208	63.7537	11.1220	421	8.7	80.2	8.7	2.4	0.0	0.0	1.4	0.0	19.3	41.3	24.8	16.5	3.0
209	63.7157	11.1205	30	2.9	57.9	22.3	10.9	2.5	3.5	0.4	0.0	6.3	14.5	42.5	22.6	3.6
210	63.7266	10.9822	425	9.8	88.1	2.1	0.0	0.0	0.0	0.8	0.0	20.9	37.5	19.1	19.0	4.2
211	63.7559	10.9887	416	11.5	87.1	1.4	0.0	0.0	0.0	1.0	0.0	33.1	46.1	16.3	15.6	4.3
212	63.7129	10.8874	426	10.7	87.7	1.6	0.0	0.0	0.0	1.1	0.0	23.5	47.4	17.4	13.6	2.7
213	63.6887	10.8005	412	10.6	87.3	2.1	0.0	0.0	0.0	1.9	0.0	25.5	42.5	17.0	15.2	4.4
214	63.6568	10.8284	72	2.6	41.4	36.2	14.6	2.2	3.1	3.8	0.0	6.9	19.3	33.2	19.6	6.5
215	63.6711	10.7238	370	11.1	87.4	1.5	0.0	0.0	0.0	2.2	0.0	20.8	47.0	20.2	16.0	3.0
216	63.6227	10.6901	175	4.5	47.9	25.9	13.1	4.5	4.1	3.7	0.0	20.1	30.7	30.5	16.2	3.5
217	63.6080	10.5619	212	2.3	17.0	4.3	20.5	27.7	24.1	14.5	4.4	6.3	15.9	19.5	27.3	4.6

Table S3 - continued

Sampling station	Latitude	Longitude	Water depth	< 2 µm	2-63 µm	63-125 µm	125-250 µm	250-500 µm	500-2000 µm	Calcite	Aragonite	Sum Illit + Mica	Sum Phyllosilicates	Quartz	Plagioclase	K-feldspar
	(DD)	(DD)	(m)	(%)	(%)	(%)	(%)	(%)	(%)	(%)	(%)	(%)	(%)	(%)	(%)	(%)
300	63.5885	10.4822	253	9.7	83.2	4.0	3.0	0.1	0.0	3.0	0.0	21.3	39.3	20.0	16.6	3.6
301	63.5641	10.5268	176	7.4	71.4	12.7	6.0	2.1	0.5	2.8	0.0	17.4	28.5	22.9	25.9	2.9
302	63.5349	10.4954	165	8.0	79.4	9.9	2.7	0.0	0.0	1.2	0.0	20.4	32.0	21.7	22.4	2.3
303	63.5610	10.3484	240	8.7	78.2	9.6	3.4	0.1	0.0	1.7	0.0	12.3	36.0	21.6	15.8	6.0
304	63.5475	10.7542	63	5.8	74.5	14.9	4.8	0.0	0.0	0.6	0.0	10.0	20.9	26.8	26.8	4.9
305	63.5521	10.8345	62	5.7	85.7	6.4	2.2	0.0	0.0	0.6	0.0	22.8	34.7	22.7	15.1	2.4
306	63.5791	10.8429	117	10.5	88.8	0.7	0.0	0.0	0.0	0.5	0.0	21.0	47.9	14.3	14.7	2.8
307	63.4956	10.6603	173	8.8	90.4	0.8	0.0	0.0	0.0	0.4	0.0	29.5	44.8	12.8	16.0	2.6
308	63.4872	10.7320	82	4.4	87.0	6.1	2.5	0.0	0.0	0.9	0.0	13.6	30.5	27.1	22.1	5.1
309	63.4602	10.8520	77	4.7	87.5	5.6	2.2	0.0	0.0	0.9	0.0	15.5	31.4	26.2	25.3	3.1
310	63.4346	10.7829	58	5.1	88.3	5.0	1.7	0.0	0.0	0.5	0.0	9.0	24.6	28.3	27.2	4.2
311	63.4624	10.6616	177	8.1	90.8	1.1	0.0	0.0	0.0	0.4	0.0	11.7	33.9	20.0	23.4	1.0
312	63.4661	10.5415	254	9.0	89.5	1.5	0.0	0.0	0.0	0.7	0.0	15.2	30.9	18.5	24.4	3.7
313	63.4743	10.4608	316	8.4	84.3	4.7	2.6	0.0	0.0	0.0	0.0	14.0	32.9	19.8	19.8	3.1
314	63.4411	10.3736	71	3.1	49.4	16.5	14.9	8.6	7.5	0.4	0.0	11.7	29.9	32.1	20.1	4.7
315	63.4723	10.2674	492	6.6	71.2	15.6	6.6	0.0	0.0	0.7	0.0	17.8	35.0	28.4	18.4	5.1
316	63.5072	10.2681	483	9.0	89.0	2.0	0.0	0.0	0.0	1.5	0.0	22.5	35.8	17.2	16.4	3.5
317	63.5436	10.2457	292	8.8	74.8	6.5	8.0	1.6	0.3	1.4	0.0	16.4	41.8	17.2	19.8	2.9
318	63.5052	10.1794	500	7.9	89.7	2.4	0.0	0.0	0.0	1.8	0.0	19.6	39.7	19.2	17.6	4.1
319	63.4771	10.1936	504	7.4	85.4	5.6	1.6	0.0	0.0	2.9	0.0	5.8	23.6	26.0	18.3	4.5
320	63.4517	10.1248	500	7.8	90.2	2.1	0.0	0.0	0.0	3.8	0.0	17.7	29.7	23.9	17.2	4.2
321	63.4686	10.0443	512	6.4	77.2	11.7	4.7	0.0	0.0	3.1	0.0	21.4	33.5	21.9	20.0	3.4
322	63.4029	10.0158	433	7.0	90.4	2.6	0.0	0.0	0.0	2.8	0.0	25.2	41.6	20.3	15.8	4.7
323	63.3586	10.0596	335	6.2	92.1	1.7	0.0	0.0	0.0	0.0	0.0	23.5	37.3	21.8	19.7	3.5

Table S3 - continued

Sampling station	Latitude	Longitude	Water depth	< 2 µm	2-63 µm	63-125 µm	125-250 µm	250-500 µm	500-2000 µm	Calcite	Aragonite	Sum Illit + Mica	Sum Phyllosilicates	Quartz	Plagioclase	K-feldspar
	(DD)	(DD)	(m)	(%)	(%)	(%)	(%)	(%)	(%)	(%)	(%)	(%)	(%)	(%)	(%)	(%)
324	63.3311	10.1693	170	3.1	73.0	15.7	7.2	0.7	0.3	0.0	0.0	23.5	36.2	30.5	20.3	2.4
325	63.3432	9.9087	301	4.4	81.0	9.8	4.7	0.1	0.0	0.0	0.0	16.6	32.5	25.0	18.4	3.8
326	63.4755	9.9337	530	6.5	75.8	12.9	4.8	0.0	0.0	1.9	0.0	20.5	39.4	20.7	18.5	2.4
327	63.5279	9.8733	546	5.5	67.1	14.3	11.2	1.7	0.2	4.0	0.0	20.5	31.9	25.6	18.7	5.2
328	63.5736	9.8417	566	5.6	73.9	12.7	6.7	0.9	0.2	3.9	0.0	20.0	32.4	21.2	21.8	5.8
329	63.6251	9.7759	605	3.5	52.9	4.6	8.1	17.3	13.7	3.8	1.6	16.1	30.8	21.7	12.0	2.9
400	63.7080	9.8546	225	5.6	66.1	19.7	8.6	0.0	0.0	3.7	0.0	17.6	31.4	18.7	18.1	3.7
401	63.7101	9.8621	225	6.2	80.3	9.4	3.6	0.4	0.1	4.6	0.0	10.9	20.1	18.9	30.0	7.5
402	63.7226	10.0101	83	3.8	78.1	13.5	4.6	0.0	0.0	4.8	0.0	19.6	34.5	18.2	17.4	3.4
403	63.7607	10.0419	94	4.7	75.9	12.3	5.3	1.1	0.7	3.5	0.0	9.3	23.2	25.2	22.9	3.4
500	63.6841	9.7277	115	2.4	25.0	19.2	26.3	10.6	16.5	10.3	5.9	5.3	11.7	27.7	20.3	5.8
501	63.6525	9.6666	389	2.7	41.8	32.5	20.3	2.5	0.3	9.0	3.8	7.7	18.8	27.8	17.3	5.0
502	63.5941	9.4771	350	3.2	32.2	15.7	27.7	14.0	7.2	9.1	6.0	10.7	18.5	22.8	19.1	5.3
			mean	6.6	83.1	5.9	2.7	0.0	0.0	1.1	0.0	19.6	34.7	21.4	19.5	3.6
			s.d. [(a)]	2.8	17.6	7.8	6.6	5.0	4.4	2.7	1.3	6.9	9.7	5.7	3.8	1.3
									Error (rel.%)	±1	±2-3	±5	±5	±1	±2-5	±2-5

[(a)] s.d. = standard deviation (1 sigma)

[(b)] Samples containing aragonite are mark in grey

Table S4: Results of the PCA used to calculate the TM index. Variables are $\delta^{13}C_{org}$ and the fraction of terrestrial organic carbon (F_{terr})

Sampling station	Factor scores: F1	Factor scores: F2
100	-1.79	-0.45
101	-0.66	0.51
102	-0.39	0.27
103	-0.19	-0.01
104	-0.92	0.88
200	-0.40	0.14
201	-1.29	0.38
202	-1.54	-0.12
203	-1.44	-0.15
204	-2.29	-0.63
205	-2.28	-0.31
206	-0.96	-0.13
207	-1.90	-0.67
208	-0.73	-0.09
209	-2.81	0.23
210	-0.20	-0.06
211	-0.19	0.16
212	-0.34	0.08
213	-0.09	0.34
214	1.54	-0.44
215	-0.02	0.34
216	0.65	0.44
217	0.49	0.63
300	0.99	-0.03
301	1.24	-0.19
302	0.76	0.21
303	0.44	0.69
304	0.43	-0.44
305	0.15	-0.24
306	0.28	-0.09
307	0.07	0.37
308	-0.20	-0.11
309	-2.27	-0.89
310	-1.24	-0.21
311	-0.04	0.23
312	0.42	0.02
313	0.54	0.01
314	-2.69	0.96
315	0.56	0.38
316	0.88	0.17
317	1.27	-0.04
318	0.84	0.22
319	0.36	0.04
320	1.12	0.08
321	0.97	0.14
322	0.73	0.09
323	-0.60	0.14
324	-3.25	-0.36
325	-1.47	-0.44
326	1.08	-0.27
327	1.20	0.17
328	1.16	-0.07
329	-0.75	0.00
400	2.13	-0.06
401	2.23	-0.51
402	1.93	-0.44
403	1.65	-0.55
500	1.61	0.46
501	2.27	-0.47
502	2.93	-0.31

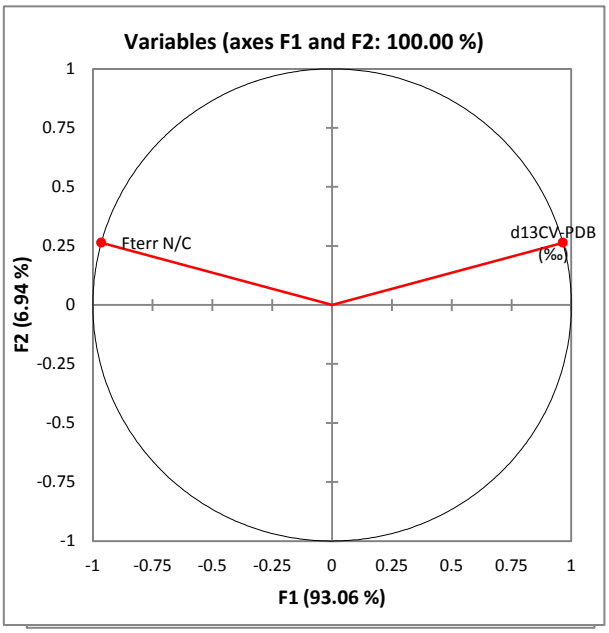

Table S5: Location of the presented bedrock samples and results of the elemental analysis

UTM E	UTM N	Rock type	Ni [ppm]	K_2O [%]	UTM E	UTM N	Rock type	Ni [ppm]	K_2O [%]
645188	7021680	Sandstone, feldspar-bearing	110	2.89	642875	7066809	Greenstone	35	0.44
641558	7021519	Metagreywacke	95	2.73	641030	7068934	Trondhjemite	8	2.63
641632	7028146	Gabbro	160	0.25	614498	7083448	Greenstone	43	0.83
644835	7031285	Gabbro	48	0.24	626138	7065705	Phyllite	61	2.58
649304	7029928	Phyllite	59	2.82	620181	7069009	Garben schist	62	2.24
618189	7029671	Mica schist	37	1.76	619476	7059312	Greenschist	133	1.31
614794	7029506	Quartzite	15	1.26	617342	7055829	Phyllite	17	1.05
613791	7033720	Phyllite	93	1.37	615843	7056711	Phyllite	28	1.19
620595	7039507	Hornblende schist	137	3.32	611108	7058801	Metagreywacke	106	2.15
630851	7037838	Diorite	57	0.16	549438	6992795	Quartz sandstone	67	1.26
617719	7042497	Metagreywacke	58	3.05	543704	6994428	Conglomerate	66	0.84
616119	7042602	Conglomerate	12	0.43	535579	6991720	Metagreywacke	8	3.69
632669	6996987	Trondhjemite	6	0.87	536587	6973767	Trondhjemite	0	3
644458	6976089	Mica schist	81	2.6	535927	6970934	Trondhjemite	0	2.78
647922	6979264	Mica schist	41	2.1	538369	6967138	Hornblende schist	111	2.42
655295	6983875	Granite	0	5.11	539600	6981706	Greenstone	78	0.94
657027	6986490	Granite	0	4.72	531738	6980998	Trondhjemite	0	0.54
639453	6985033	Mica schist	61	2.85	526048	7004681	Mica schist	43	1.28
640705	7007508	Metapelite	69	2.68	528604	7008646	Mica schist	95	2.03
646215	7002010	Mica schist	44	2.07	535578	7000663	Greenstone	70	0.19
643205	6999502	Amphibolite	111	0.2	553653	6978306	Phyllite	11	1.2
635774	6990308	Mica schist	49	1.95	560616	6994257	Quartz sandstone	29	0.45
618618	7000670	Mica schist	177	3.12	562262	6996882	Quartz sandstone	34	1.95
614180	7000104	Mica schist	195	3.31	557922	6952945	Phyllite	39	2.79
612362	7005961	Mica schist	16	3.54	552185	6947400	Metagreywacke	60	2.83
607211	7009906	Hornblende schist	140	2.24	555131	6941829	Mica schist	39	3.02
597507	7010404	Phyllite	42	1.7	560024	6930983	Mica schist	118	1.53
677647	7121405	Sandstone, feldspar-bearing	5	6.13	560929	6932619	Mica schist	22	1.68
683852	7120557	Phyllite	31	4.43	575148	6938832	Mica schist	179	3.51
662781	7113302	Phyllite	84	2.34	572260	6941301	Mica schist	13	2.12
666479	7117786	Phyllite	61	1.77	569079	6938612	Mica schist	53	3.17
654158	7120648	Rhyolite	0	5.26	564056	6944155	Mica schist	78	1.38
660120	7126308	Limestone	0	0.521	571446	6929320	Mica schist	240	4.68
672237	7135177	Greenstone	66	1.71	572397	6926283	Mica schist	67	2.42
662238	7131649	Greenstone	227	0.83	618906	6965795	Amphibolite	12	0.14
565811	7036241	Granitic gneiss	0	1.62	583173	6962655	Mica schist	16	3.14
562423	7024523	Greenstone	63	0.1	584457	6957862	Mica schist	46	2.7
565820	7028590	Greenstone	130	0.05	576426	6967119	Mica schist	24	1.62
585457	6981171	Mica schist	94	0.56	576112	6971793	Mica schist	44	3
612036	6973158	Mica schist	398	3.14	575091	6983736	Mica schist	40	1.9
600025	6983066	Mica schist	38	1.98	631682	6968183	Garben schist	71	2.82
596942	6984770	Diorite	0	2.26	628262	6967686	Mica schist	70	1.76
540060	6945326	Quartzite	11	1.46	609046	6979067	Mica schist	190	3.38
552036	6970756	Quartzite	0	0.84	573986	6987421	Mica schist	112	1.4
548793	6953013	Granodiorite	84	1.08	554034	6975900	Phyllite	42	1.78
542502	6950474	Trondhjemite	15	2.26	553246	6977237	Phyllite	29	2.29
558937	6978263	Phyllite	125	2.28	563141	6985613	Metagreywacke	65	0.91
556885	7009074	Greenstone	110	0.18	594233	7055171	Slate	50	2.31
539034	7019919	Mica schist	11	0.29	594763	7059166	Metagreywacke	8	3.1

Table S5 - continued

UTM E	UTM N	Rock type	Ni [ppm]	K2O [%]	UTM E	UTM N	Rock type	Ni [ppm]	K2O [%]
542960	7051225	Granitic gneiss	0	6.34	566883	7007844	Metagreywacke	10	1.98
560850	7061972	Granitic gneiss	5	3.62	582127	6998738	Mica gneiss	10	1.91
559610	7046353	Mica schist	47	2.02	574096	6999590	Mica gneiss	75	3.05
558886	7050541	Mica schist	98	4.26	568195	7001346	Phyllite	70	1.97
548789	6935163	Mica schist	12	1.13	644459	7051600	Phyllite	17	0.46
544294	6930090	Phyllite	29	1.86	646254	7048778	Metasandstein	28	1.44
547533	6928148	Mica schist	163	2.8	593929	7044906	Greenstone	66	0.32
552681	7024343	Mica schist	53	1.72	589877	7041717	Metasandstein	53	1.65
606247	7038278	Carbonaceous phyllite	47	2.72	605036	7040702	Slate	18	3.22
590696	7032150	Mica schist	15	1.51	603968	7025311	Greenstone	24	0.18
595460	7018957	Greenstone	227	0.72	608304	7018480	Mica schist	74	2.23
540544	7044219	Greenstone	26	0.35	604696	7015717	Mica schist	68	1.85
544874	7037108	Granodioritic gneiss	8	3.92	590589	7023717	Greenstone	28	1.12
548317	7034320	Mica gneiss	19	3.68	588742	7012785	Carbonaceous phyllite	56	2.6
533388	7017160	Arkose	12	3.38	596262	7003841	Mica schist	44	1.2
613485	7094887	Greenschist	65	2.57	604906	7000827	Mica schist	40	3
609119	7091151	Greenschist	61	0.19	569731	7021750	Metagabbro	85	0.06
603698	7085791	Mica schist	22	1.76	572403	7009327	Greenschist	349	0.08
600460	7083602	Granite	0	2.95	607064	6989266	Migmatite	41	2.05
596978	7072270	Mica schist	69	2.03	644340	7117876	Rhyodacite	0	5.35
593387	7078490	Phyllite	64	2.23	648233	7119662	Rhyolite	5	4.85
580448	7067722	Mica schist	19	1.12	669836	7131945	Marble	0	0.015
584344	7064645	Mica schist	69	3.16	642622	7121754	Carbonaceous sandstone	0	0.19
563560	7048358	Mica schist	45	1.86	660457	7132490	Greenschist	82	0.1
611055	7114910	Granitic gneiss	0	5.95	645213	7122667	Sandstone	9	1.64
588300	7085144	Granodioritic gneiss	0	2.67	624066	7113046	Carbonaceous sandstone	12	2.02
601259	7103885	Diorite	11	1.95	625077	7111204	Carbonaceous sandstone	12	3.03
603140	7102075	Quartz sandstone	11	2.02	592594	6967789	Phyllite	50	0.58
628640	7092524	Quartz sandstone	33	4.39	591828	6968689	Phyllite	27	0.74
669130	7079120	Garben schist	77	4.15	586538	6974998	Mica schist	67	2.98
666562	7077103	Quartz sandstone	27	2.38	569538	6961611	Phyllite	77	1.64
662392	7079386	Phyllite	41	1.41	567452	6974063	Quartz mica schist	84	2.68
655598	7079165	Phyllite	57	2.74	574992	6956842	Mica schist	31	0.57
646429	7080942	Phyllite	31	1.81	525012	6956637	Quartz schist	6	3.82
643891	7085468	Rhyolite	0	5.89	607209	6958636	Gabbro	52	0.52
639722	7077692	Greenstone	23	0.6	607603	6964921	Gabbro	37	0.51
660168	7062329	Gabbro	31	1.22	611959	6967761	Phyllite	161	3.41
656335	7062564	Carbonaceous phyllite	69	2.73	652275	7093987	Greenstone	56	0.08
645463	7065972	Diorite	60	0.16	648437	7097519	Metadacite	0	4.83
622354	7097936	Metaarkose	11	4.41	631428	7098266	Mica schist	34	3.75
552847	6917668	Mica schist	102	1.3	633228	7111398	Greenschist	38	1.02
640005	7104785	Metarhyodacite	0	5.33					